CHALMERS

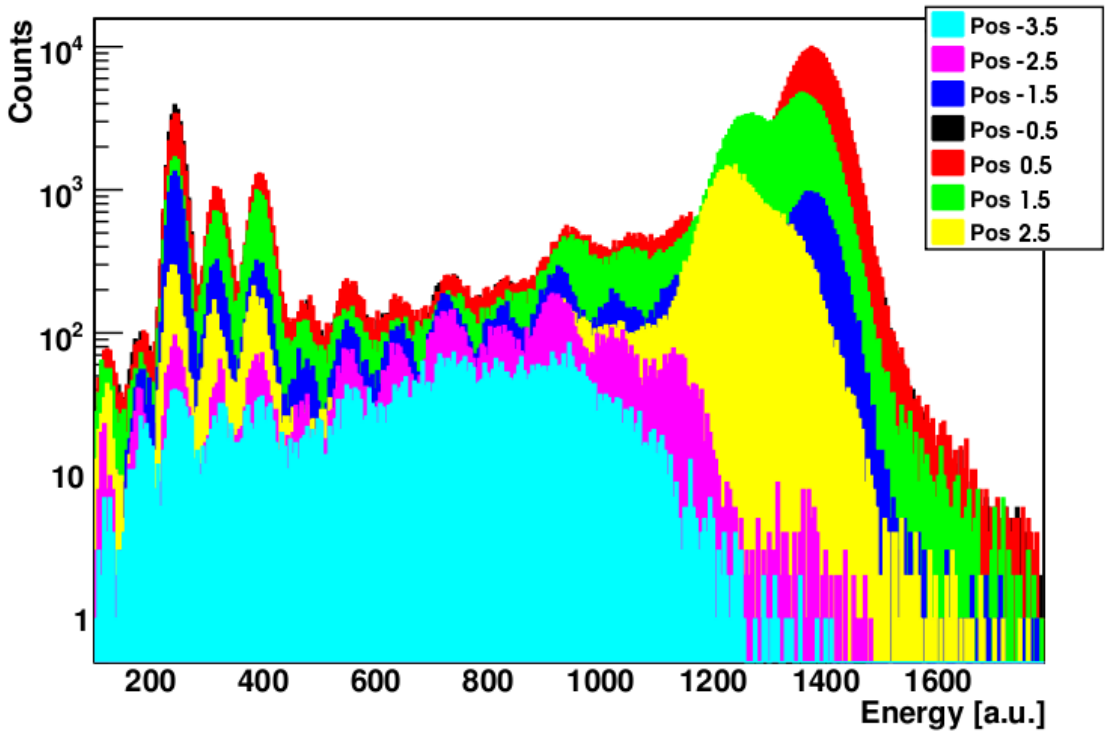

Optimised Use of Detector Systems for Relativistic Radioactive Beams

How to kill a smiley and get away with it!

Master Thesis in Fundamental Physics

SIMON LINDBERG

Department of Fundamental Physics
CHALMERS UNIVERSITY OF TECHNOLOGY
Göteborg, Sweden, 2013

Thesis for the Degree of Master of Science

Optimised Use of Detector Systems for Relativistic Radioactive Beams

How to kill a smiley and get away with it!

Simon Lindberg

Supervisors:

Håkan Johansson
Andreas Heinz

Department of Fundamental Physics
Chalmers University of Technology
Göteborg, Sweden 2013

Optimised Use of Detector Systems for Relativistic Radioactive Beams
How to kill a smiley and get away with it!
Simon Lindberg

Department of Fundamental Physics
Chalmers University of Technology
SE-412 96 Göteborg
Sweden
Telephone + 46(0)31-772 1000

Cover: The energy spectra at different positions in a long plastic scintillator used in the NTF detector after a correction has been applied to the data. The different colours represent different positions in the paddle according to the legend. Position 0 is in the middle of the paddle and the PMTs are positioned at position -4 and 4, respectively.

Chalmers Reproservice
Göteborg, Sweden 2013

Optimised Use of Detector Systems for Relativistic Radioactive Beams
How to kill a smiley and get away with it!
Simon Lindberg
Department of Fundamental Physics
Chalmers University of Technology

Abstract

Ever since the discovery of the atomic nucleus, the exploration and understanding of its properties has been a frontier of physics research. Such investigations are still ongoing at different research facilities around the world. One of these places is the GSI accelerator laboratory where experiments with unstable heavy ions are performed. To obtain high-quality results from the experiments, it is essential that the detectors used are performing at their maximum. Hence it is important to understand the characteristics of the detectors to be able to find and correct errors.

In this thesis, the response of two different detector systems in the LAND-setup at GSI is investigated. The first detector system is called the Crystal Ball, a γ-detector, which is also able to detect high-energy protons. The second detector type is used for detecting ions. It consists of a long plastic scintillator which is very common in nuclear physics experiments and is used in several different detector systems in the LAND-setup. For the Crystal Ball an evaluation of different addback routines were performed. An addback routine is a method to recreate the multiplicity and energy of γ-rays and protons hitting the Crystal Ball detectors. This was done based on simulations of different scenarios.

For the scintillator, experimental data were used. The motivation to investigate the behaviour of the scintillator is a feature causing the detector to respond differently depending on the position of a hit in the paddle. The origin of this behaviour was found and different methods for correction are suggested and evaluated.

The third and last topic of this thesis is a brief analysis of data collected by a detector system constructed to find a relation between energies deposited by cosmic muons and protons in the Crystal Ball. With this relation it is possible to calibrate the Crystal Ball for a range of proton energies, using cosmic muons. The results from the experiment agree with expectations, however to find the relation, a more thorough analysis is needed.

Contents

1 Introduction

The history of nuclear physics starts with the studies of the properties of the atoms and the discovery of radioactivity. Due to the observations of nuclear scattering, Rutherford in 1911 proposed that the atom consists of a nucleus with positive charge and electrons with negative charge circling around the nucleus at a far distance [1]. With the discovery of the atomic nucleus the study of their behaviour was initiated and the scientific area known as nuclear physics was born.

The last century, many different important discoveries have been made within the nuclear physics area. Both for theoretical understanding, but also for practical use, such as x-ray, radiotherapy and nuclear power. One of the most fundamental discoveries was the finding of the neutron. This led to the model of the atomic nucleus which is in use today. Despite much progress there are still areas which are not fully explored. One important area is the structure of nuclei. By understanding how the nucleus is built up and how it is kept together many questions can be answered, such as what happens in a star, what limits the mass of the nuclei and many more.

To learn about nuclear structure, exotic nuclei with very many or very few neutrons relative to the number of protons are created in accelerators. Many of the isotopes used for these studies can only be created in accelerators. That is one reason why most of the experiments in nuclear physics are carried out at accelerator facilities. One such facility is the "GSI Helmholtzzentrum für Schwerionenforschung" (GSI) situated north of Darmstadt in Germany. Here many nuclear physics experiments take place, especially with heavy nuclei [2]. In the fragment separator (FRS) the unwanted isotopes are separated from the beam giving a beam with only the desired isotope. This beam is distributed to the detector system used for the experiment. In this thesis the LAND-setup has been used.

When performing experiments there are always uncertainties involved in the results due to the unavoidable errors in the measurements. In order to obtain as good results as possible, it is essential to minimise the measurement errors. The problem is that the errors not always are that easy to find, and even if they are known, it is often tricky to correct them. The aim of this thesis is to improve the usage of the detectors in the LAND-setup. With data corrected for known errors, the measurement results can be improved, both for future experiments but also for experiments already performed.

1.1 Scintillation Detectors

A scintillation detector consists basically of two parts, one scintillator and one photon detector. It is possible to create a scintillator of many different materials and it can be either gaseous, liquid or solid [3]. Which material is used depends on the desired properties of the detector. The purpose of the scintillator is to interact with ionising particles, transforming their kinetic energy into photons. For identical types of particles, the light produced in the scintillator is proportional to the energy loss of the particle when traversing the scintillator. The light created is detected by the photon detector which in turn gives an electric signal proportional to the light produced in the scintillator. The light detector is usually a photo multiplier tube (PMT). The PMT is very sensitive to light and has the ability to increase the signal millions of times. This is done via the photo electric effect and an avalanche of secondary emission. The basic function is that a photon hits the PMT, creating an electron via the photo electric effect. The electron is accelerated towards a dynode where it emits more electrons via the secondary electron emission effect. These electrons are accelerated towards another dynode, creating even more electrons which are accelerated towards another dynode and so on. In this way the signal is increased and in the end a single photon has created a measurable electrical charge pulse. The two most commonly used materials are plastic and NaI. Scintillators made of NaI are of the type inorganic crystals and needs an activator impurity, for NaI often Tl. Plastic scintillators are of the type organic detectors which do not need any activator impurity. The main advantages of the inorganic crystal are its high stopping power and the high light output. Its main disadvantage is hygroscopicity, it has to be kept in air tight enclosures to be protected against the moisture in the air. The plastic scintillator has the advantage of being easy to handle, it has a quick response time and it can be manufactured in basically any shape.

As mentioned before there are many different types of scintillators to choose from. Each of them has its own advantages and weaknesses. In nuclear physics experiments it is usually important to have a short decay time and a high light output. The short decay time is necessary because of the short interval between events and to get a good time resolution. During an experiment the beam creating the desired nuclear reactions might only be active for some seconds at the time. In these seconds millions of events may occur. In order to be able to use as many of them as possible, the detectors need to be able to operate very quickly. The light output is important for the efficiency and the resolution of the detector. The resolution is depending on the photon statistics, the more photons the higher resolution. Another important factor which also affects the resolution is the light transport efficiency. Since the number of photons created are relatively few, it is

crucial to have as low losses as possible in order to get as much light as possible to the PMT. To minimise the losses, plastic scintillators have treated surfaces which enhance the internal reflection. The scintillator is also wrapped in a shielding and in an opaque plastic. This is to further enhance the reflection at the surface, but even more important, to avoid letting light in from outside. There is also a continuous loss of photons in the material due to interactions between the photons and the material. This loss is usually described by

$$N = N_0 \, \mathrm{e}^{-\frac{x}{f(\lambda)}}, \tag{1.1}$$

where N is the number of photons at the distance x from the creation point [4]. N_0 is the original number of photons created and $f(\lambda)$ is the wavelength dependent attenuation length, i.e. how far the signal can travel before its photon number has decreased by a factor e.

1.2 The LAND-Setup

The LAND-setup is a complex system of detectors designed to study the properties of nuclei by colliding highly energetic ions with a target. The detectors in the setup can be divided in those positioned before the target and those positioned after the target. To understand the reaction in the target it is important to know what has hit the target. By knowing the energy of the incoming beam and detecting the charge and the time of flight of the ions for a known distance, it is possible to infer what isotope each ion is. Thus the main purpose of the detectors before the target is to measure the charge and the time of flight. Depending on the experiment the setup may be altered, but its basic design [5] is shown in Fig. 1.1. The first detectors the beam passes are scintillators positioned at the ion-optical focal planes of the FRS called S2 and S8. These scintillators are used for time of flight measurement before the target. Next comes the PSP detector (Position Sensitive silicon Pin diode) which is used for beam tracking and charge measurements of the heavy ions. This is mounted together with the pixel detector which is used to calibrate the position of the PSP. To monitor the width of the beam, the ROLU (Rechts, Oben, Links, Unten) is used. It is made of four movable scintillators which are used to discriminate ions too far from the centre of the beam. After that comes the POS detector. It is a scintillator which is used both as a stop and start detector for the time of flight measurement. It stops the time that was started when the beam passed S2 and S8 but at the same time is used as start reference for a new time of flight measurement. After the beam passed a second PSP and pixel detector it hits the target inside the Crystal Ball. From these detectors described above, both the time of flight and the charge of the incoming ions are measured, hence the isotopes can be identified.

After the beam has hit the target, many different particles may be created. These need to be identified and their energy needs to be measured. The γ-rays created and protons scattered at large angles are detected by the Crystal Ball which is described in detail in Sec. 1.2.1. The particles scattered in the direction of the beam (and ions that did not react in the target) pass ALADIN (A LArge DIpole magNet) which is a magnet separating the different fragments. The particles are bent differently depending on their magnetic rigidity. Electrically uncharged particles though, are not affected and hence continue straight ahead to the LAND detector, which is a neutron detector and is described in detail in Sec. 1.2.2. Heavy charged particles are bent from their trajectories and hit the GFI detectors (Grosser FIber) which are scintillating fibre detectors used to measure the trajectories of the particles. The GFI consists of many thin scintillating fibres closely packed. When a charged particle passes through the detector the traversed fibres will give a signal. From this the position of the particle in the detector can be found and by placing two of these detectors after each other and by using the position of the target, the trajectory through the magnet can be calculated. Finally the particles hit the NTF (New Time of Flight wall) which is a scintillation detector that gives the stop signal to the time of flight measurement started by the POS detector. The NTF is also capable of measuring the charge and position of the particles. The protons scattered from the target are bent to the largest deflection angle in ALADIN due to their high charge to mass ratio. These are measured in a similar manner like the heavier charged particles. First they hit the PDC detectors (Proton Drift Chambers) used to find out their trajectories and then the TFW detector (Time of Flight Wall) which is used for the time of flight, charge and position measurements. The NTF and the TFW are described in detail in Sec. 1.2.3.

1.2.1 Crystal Ball

The Darmstadt-Heidelberg Crystal Ball is a γ-detector which has been upgraded to be able to also detect protons [5]. The name is a bit misleading since it is not really a ball but rather a shell enclosing the target. The shell is made of 162 crystals although three of them are removed, two in the beam line (front and back) and one for the support of the target. The sphere has an inner radius of 25 cm and the crystals are 20 cm thick giving an outer radius of 45 cm. The crystals are made of NaI activated with Tl creating a scintillating material. The crystals are made in four different shapes arranged in such a way that they all cover the same solid angle. The crystals are placed as in Fig. 1.2

Each crystal is labelled by an individual number ranging from 1 to 162. Seen from the beam direction the front crystal is No. 82 and the back crystal is No. 81.

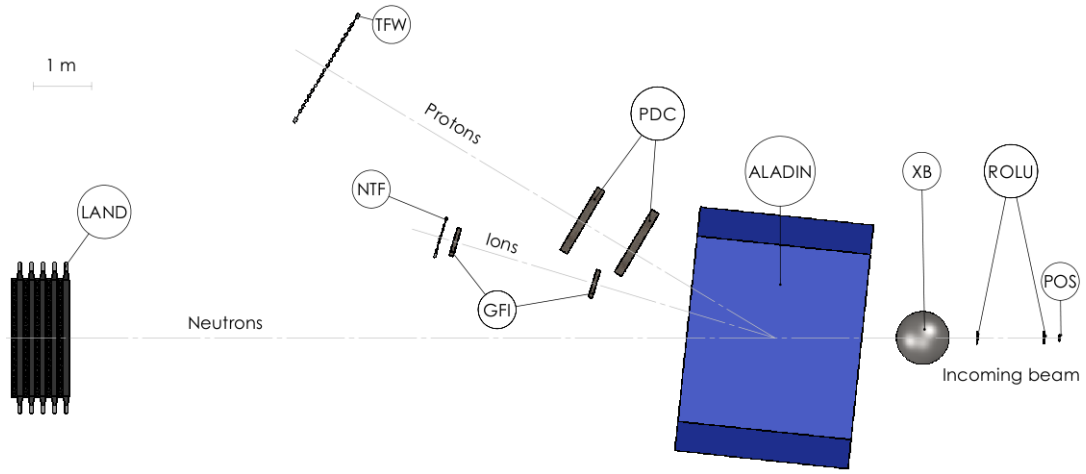

Figure 1.1: *A sketch of the LAND-setup as seen from above. The target is placed inside the Crystal Ball (XB).*

The rightmost crystal is No. 1 and the leftmost No. 162. On top is No. 86 and in the bottom is No. 77. All the crystals are arranged in such a way that the sum of two opposing crystals always is 163.

In the centre of the Crystal Ball a reaction target is placed. When the beam hits the target, γ-radiation may be emitted which the Crystal Ball can detect. Apart from the γ-radiation, other particles are emitted as well due to nuclear reactions when the beam impinges on the target. The main function of the Crystal Ball is to detect the number and energies of γ-rays and protons emitted in the reaction [7].

When a γ hits a crystal it can interact in three ways, photoelectric absorption, Compton scattering or pair production. In general the photoelectric absorption is most common for low energetic γ-rays, pair production is most common for high energetic γ-rays and Compton scattering is the dominant process in between the others [8]. In Fig. 1.3 an example of the total absorption coefficient for γ-rays together with the contribution of the different interaction

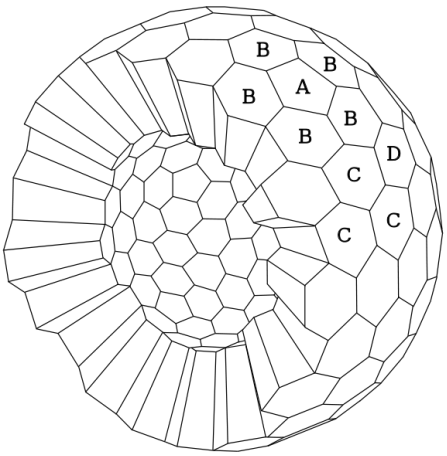

Figure 1.2: *A schematic view of the crystals building up the crystal ball. The letters mark the shape of the crystal. Figure from Ref. [6].*

types in aluminium is shown. Depending on the material the absolute numbers in the figure change, but the general pattern is maintained.
To be able to detect the correct energy of a γ, all its energy needs to be deposited

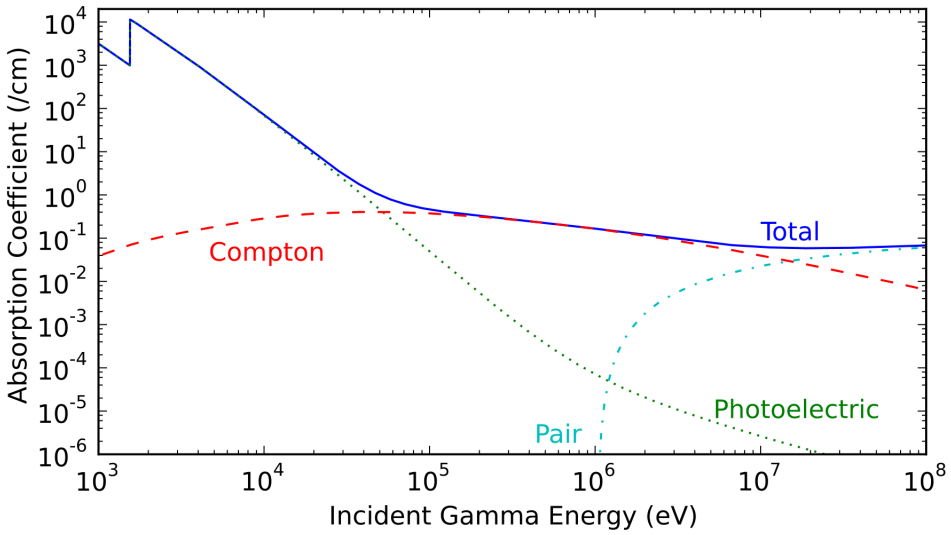

Figure 1.3: *The total absorption coefficient and the contribution from the different interaction types as a function of the γ energy. For this example Al has been used. When other materials are used the values change but the general pattern remains. Figure from Ref. [9].*

in the crystal. This is best achieved from pair production or a photoelectric absorption, since that is when all the energy is used in the reaction. The preferred case is the γ beeing absorbed via the photoelectric effect. In this case all the energy[1] of the γ is transfered to the electron. The energy of the electron is then easily detected. In the pair production all the energy of the electron is likely to be detected due to the high stopping power of electrons in the scintillator. Also the positron is stopped, but when stopped it is annihilated, creating two 511 keV photons. The photons also need to be detected in order to get the total energy of the original γ. The problem in the Crystal Ball occurs when multiple γ-rays are present in the same event and many of them are Compton scattered between different crystals. What is needed then is a so called addback routine, to match

[1] All energy except a small fraction that is used to overcome the binding energy of the electron, usually only a few eV.

the crystals together which have detected the same γ. By adding the energies detected in these crystals the total energy of the γ is obtained and also the number of γ-rays present in the event.

1.2.2 LAND & NeuLAND

LAND is an abbreviation for Large Area Neutron Detector and has given name to the entire setup used in this thesis. LAND itself has a front-face of 2×2 m^2 and is one meter deep [10]. It consists of 10 planes of scintillators, each with 20 paddles. All paddles are made of 11 sheets of iron and 10 sheets of plastic scintillators as shown in Fig. 1.4. These are put alternatively where each sheet is 5 mm thick except for the first and last sheet of iron which only are 2.5 mm. At each end of the paddle a PMT is mounted. The paddles in each plane are mounted perpendicular to each other which makes it possible to get the position of the incident neutron in both vertical and horizontal directions. The function of the iron sheets is to contribute a better material for the neutrons to interact with. A better material in this case means a material with higher proton number thus getting a higher cross-section for neutron interactions. When the neutrons interact with the nuclei, other charged particles are created which are detectable in the plastic scintillator. The position of the neutron is calculated by the time difference[2] of the signals between the two PMTs. The energy of the neutron is calculated from the position and the time of flight. A sketch of the LAND detector is shown in Fig. 1.5.

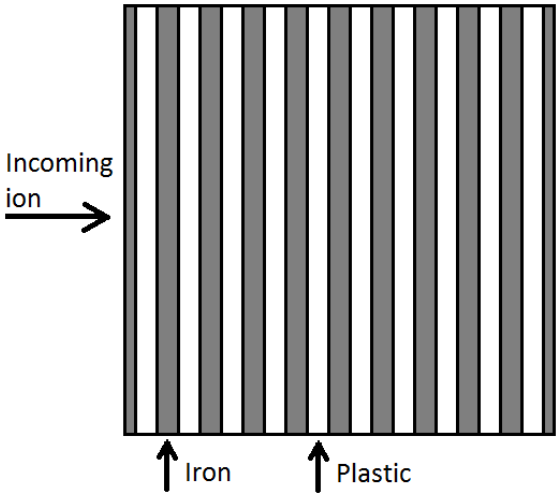

Figure 1.4: *A cross-sectional view of a paddle used in the LAND detector. The first and last iron sheets are 2.5 mm thick while the rest are 5 mm.*

LAND is planned to be replaced in the future by NeuLAND. It is supposed to fulfil the same purpose as LAND but with a higher efficiency and resolution. NeuLAND will also be bigger than its predecessor. The detector will be built by 3000

[2]The speed of light in the scintillator is about 60% of that in vacuum giving time differences in the order of ns, which are detectable.

scintillators giving the total size 2.5×2.5 m^2 with a depth of 3 m [11]. NeuLAND will be built in a way that it will be possible to divide it into two independent sections which can be moved apart, giving two detectors, each with a depth of 1.5 m. Unlike LAND, NeuLAND will only consist of scintillating material and thus no iron will be inserted. Tests and simulations have been performed for the new detector showing that a time resolution of $\sigma(\mathrm{t}) \leq 150$ ps and a position resolution of $\sigma(\mathrm{x,y,z}) \approx 1.5$ cm is possible. The first realistic tests were performed during November 2012 with a prototype consisting of 146 bars. The main purpose of the tests was to get the first experimental data on the time and position resolution. These tests are described in Chap. 4. The final detector is scheduled to be operational in 2016.

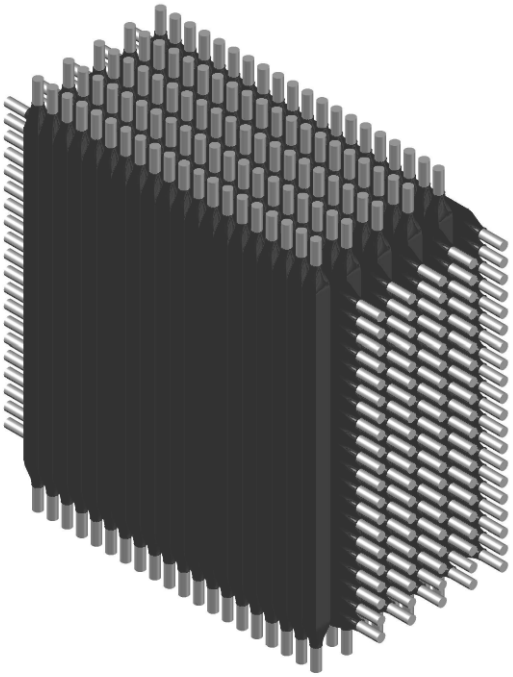

Figure 1.5: *A basic model of the LAND-detector. Each paddle is 2 meter long and 10 cm wide. It has 10 planes, each 10 cm thick.*

1.2.3 TFW & NTF

The function of the TFW and the NTF is the same. The TFW is nowadays usually used for the protons while the NTF is used for the unreacted ions and fragments. The TFW is the bigger of them, consisting of 18 plus 14 scintillating detectors.

The first 18 scintillators are mounted vertically side by side and the other 14 are mounted horizontally in front of the vertical plane. The scintillators are 10 cm wide, 0.5 cm thick and the horizontal ones are 189 cm long while the vertically mounted are 147 cm long. The NTF is built up in the same way, but is only consisting of 8 plus 8 scintillators. These are 6 cm wide, 0.5 cm thick and 48 cm long. For both the detectors the horizontally mounted bars build up the plane referred to as the y-plane (giving the y-position by the number of the bar), while the vertically mounted is the x-plane (giving the x-position by the number of the bar).

The position of a hit is calculated in the same way as in LAND, i.e. the time difference between the two PMTs gives the hit position. Also the energy is measured, giving information of which ion has been detected. If ions with the same velocity but different charge hit any of the detectors, they will deposit a different amount of their energy, thus making it possible to distinguish the charge of an ion that has hit the detector. This will be shown and used in Chap. 3.

2 Crystal Ball Addback Routines

As mentioned in Sec. 1.2.1, the γ-rays hitting the Crystal Ball can be Compton scattered between different crystals. As long as only one γ hits the Crystal Ball in each event it is no problem, but during experiments there will be several γ-rays in each event and also other particles such as protons and neutrons. Since the crystals themselves cannot decide where the γ comes from a so-called addback routine is needed. The aim of the addback routine is to add the energy from all the crystals that have energy contributions originating from the same γ. In this way the total energy deposited by it and also the number of γ-rays that have hit the Crystal Ball is obtained. The problem with the addback routine is that it should be able to follow a scattered γ till its end, but at the same time it should not add crystals which have been hit by other γ-rays. An example of what can happen in the Crystal Ball is shown in Fig. 2.1. The worst case scenario is if the same crystal has been hit by different γ-rays, because then it is not possible to distinguish between the different γ-rays. To evaluate different addback routines and compare their efficiency some simulations have been done.

2.1 Simulations

All the simulations are made with ggland[3] for Geant3[4] [12]. Each Monte Carlo simulation is done in vacuum and with 100000 events. There have been no background contributions and no energy resolution has been considered in any simulation. For the initial tests the gun[5] is fixed to shoot at crystal No. 1. This is a good choice since the removed crystals (77, 81 and 82) are far away and none of them are in the straight back-scattering angles.

One thing which was discovered was the pattern in the energy distribution for low energy γ-rays. When shooting γ-rays at crystal No. 1, a sharp line appeared for crystals with higher number, like the one in Fig. 2.2. This can be explained with Compton scattering against electrons and the energies correspond well to the

[3] A simulation tool for the LAND-setup developed by Håkan Johansson.
[4] A simulation program describing elementary particles passage through matter.
[5] The gun is the simulation parameter deciding the properties of the incident particle

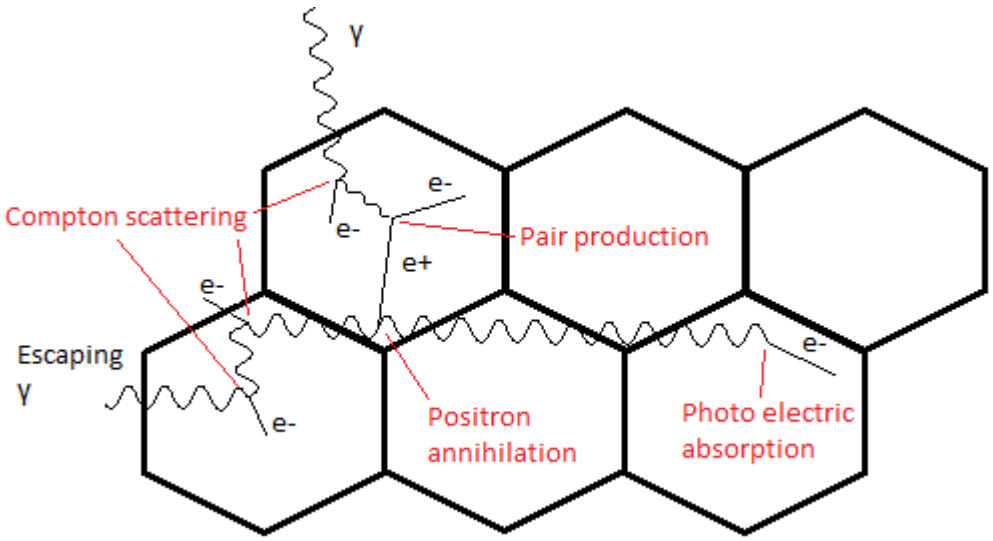

Figure 2.1: *A principal figure of what can happen in the Crystal Ball. A γ entering the crystal is Compton scattered and then produces an electron-positron pair. The e^- is stopped in the crystal and when the e^+ is stopped it is annihilated producing two new γ-rays. One is Compton scattered before escaping the bottom left crystal. The other is photo electrically absorbed in the bottom right crystal. This means that energies have been deposited in the top left, bottom left and bottom right crystals. The closest result from an addback routine would be if these three crystals were added, but because both an e^- from Compton scattering and a γ escaped not all energy has been deposited in the detectors, thus it is not possible to recreate the correct energy.*

Compton scattering equation

$$\cos\theta = m_e\left(\frac{1}{E_i} - \frac{1}{E_s}\right) + 1, \qquad [8]$$

where E_i is the initial energy of the γ, E_s is the γ energy after the scattering and θ is the scattering angle. For higher energies, $E_i > 4$ MeV the back-scattering can no longer be observed. The number of back-scattered γ-rays is shown in Tab. 2.1.

For protons there were no patterns in the scattering, but the punch-through energy is found to be around 280 MeV. This is shown in Fig. 2.3 where a clear trace is seen dropping after 280 MeV. This means that the crystals do not have sufficient stopping power for protons with energies above 280 MeV resulting in problems to detect their actual energy.

Nor for the neutrons, any patterns in the scattering could be observed. What

Table 2.1: *The number of back-scattered γ-rays for different energies. E_γ is the energy of the incident γ, the given intervals are the energies required of the scattered γ for a back scattering to be possible.*

Energy, E_γ [MeV]	Interval $E_{s,\mathrm{low}}$–$E_{s,\mathrm{high}}$ [MeV]	Amount in %
1	0.2–0.3	3.3
2	0.22–0.32	2.4
4	0.25–0.35	1.8

can be seen though, is that high amounts of energy are created when shooting 300 MeV neutrons. As shown in Fig. 2.4, no energies higher than 250 MeV are present for 250 MeV neutrons. For 300 MeV neutrons on the other hand, energies as high as ~ 600 MeV are observed. This is probably no physical phenomenon but more likely some problem with the simulation[6].

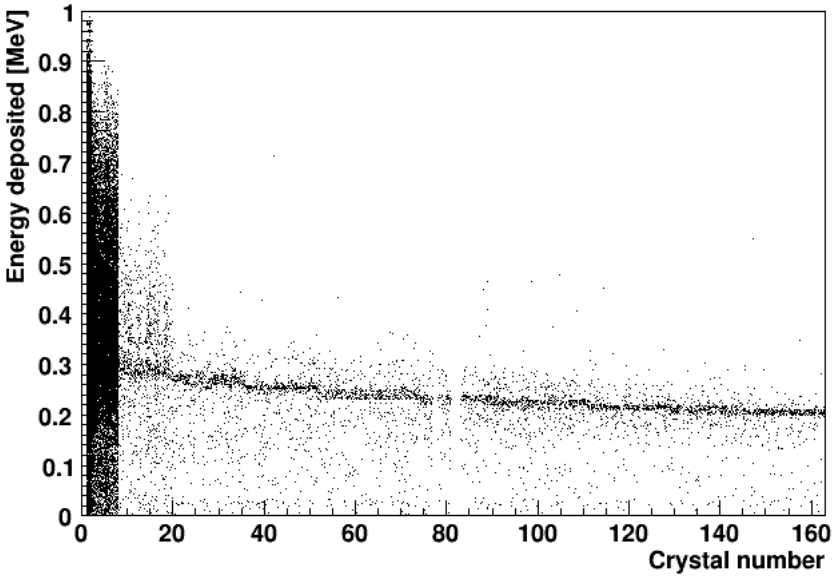

Figure 2.2: *The energy distribution for the crystals when shooting 1 MeV γ-rays in the middle of crystal No. 1. Crystal No. 2–7 are neighbours of crystal No. 1 and No. 8–19 are second neighbours, i.e. neighbours to the neighbours.*

To get an understanding why one addback algorithm might be better than another some information might be of interest. To start with, how many crystals

[6]Investigations of the complete secondary particle generation for individual events show very strange features.

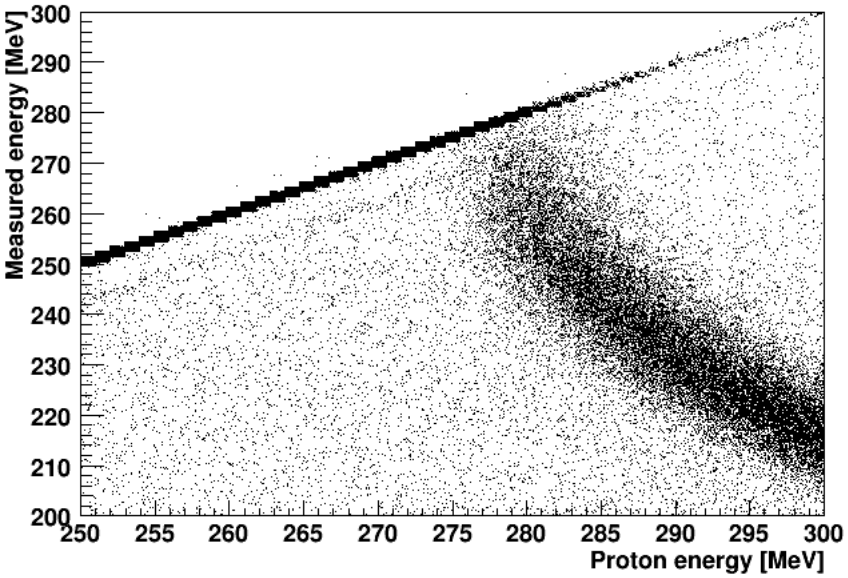

Figure 2.3: *The energy deposited in the Crystal Ball in each event plotted against the energy of the incident proton. The punch-through energy is seen at about 280 MeV. The punch-through limit is rather distinct even though some protons are completely stopped also beyond the limit.*

are hit in each event at different energies. For 100000 simulated events with a gun pointing in a random direction, the result is shown in Tabs. 2.2, 2.3 and 2.4 for γ-rays, protons and neutrons, respectively.

Another thing that was investigated was how common it is to have events where there is a space between two hit crystals. Also this was done with a random pointing gun but with a full Crystal Ball i.e. also crystals No. 77, 81 and 82 was simulated. The result from this is shown in Tab. 2.5.

Furthermore the number of times the entire energy of the particles is deposited in the detector has been extracted. For neutrons this is difficult to tell because the nuclear reaction is causing extra energy to appear as shown in Fig. 2.4, but one can assume that the occurrence of full-energy deposits is low[7]. For γ-rays and protons the results are shown in Tab. 2.6.

Another thing that has been investigated is how often the first crystal that is hit also is the one with the highest energy. This has been done for γ-rays shot

[7]The neutron's lack of electric charge makes it hard to detect because it only interacts via the strong force which gives a small cross-section. [3]

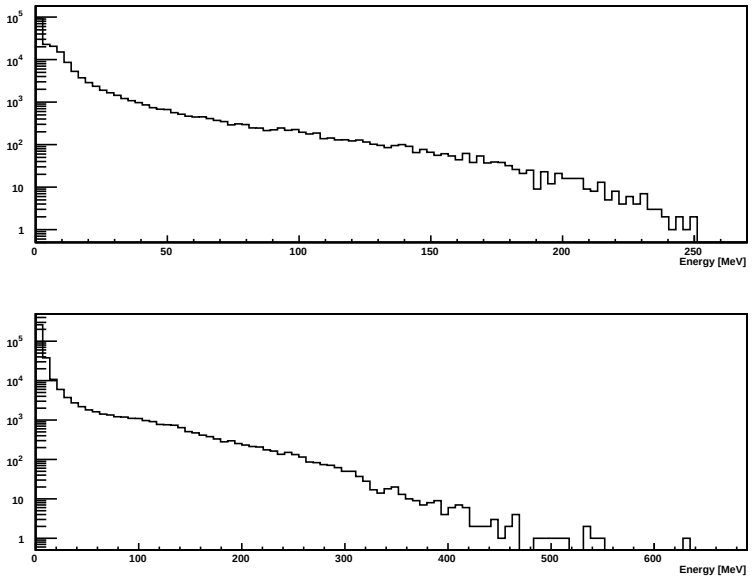

Figure 2.4: *The energy deposited in crystals by 250 MeV neutrons (upper) and 300 MeV neutrons (lower). The extra energy appearing in the lower histogram is suspected to originate from problems in the simulations.*

in the centre of a crystal, at the edge of a crystal and in the corner of a crystal. The result is presented in Tab. 2.7. The same has been performed for protons and neutrons but only when shooting in the centre of a crystal. The result of this is shown in Tab. 2.8.

Table 2.2: *The average number of crystals hit in each event for different energies of the incident γ-rays together with the number of crystals that have been hit in percent. The simulations have been done with a total of 100000 events. Events where no crystals are hit have been omitted. Bold numbers indicate the highest percentage for that energy.*

Energy	Av. cr. hit	Events in %					
E_γ [MeV]	Number	1 hit	2 hits	3 hits	4 hits	5 hits	>5 hits
1	1.4	**60.0**	32.1	4.0	0.2	0.0	0.0
2	1.6	**49.7**	34.9	7.4	0.9	0.1	0.0
5	2.0	33.1	**35.6**	15.8	4.3	1.0	0.2
10	2.4	19.8	**33.0**	23.4	10.1	3.5	1.5
20	3.2	9.3	23.5	**27.3**	18.0	8.9	6.7
30	3.7	5.6	16.3	**25.1**	21.7	13.4	12.5

Table 2.3: *The average number of crystals hit in each event for different energies of the incident protons together with the number of crystals that have been hit in percent. The simulations have been done with a total of 100000 events. Events where no crystals are hit have been omitted. Bold numbers indicate the highest percentage for that energy.*

Energy	Av. cr. hit	Events in %					
E_p [MeV]	Number	1 hit	2 hits	3 hits	4 hits	5 hits	>5 hits
1	1.0	**97.7**	0.0	0.0	0.0	0.0	0.0
10	1.0	**97.5**	0.1	0.0	0.0	0.0	0.0
50	1.0	**95.1**	1.8	0.2	0.1	0.1	0.1
100	1.2	**89.1**	5.5	0.8	0.6	0.4	1.2
200	1.6	**75.1**	12.7	2.4	1.7	1.3	4.3
300	2.6	**62.1**	14.3	3.6	2.9	2.4	12.3

Table 2.4: *The average number of crystals hit in each event for different energies of the incident neutrons together with the number of crystals that have been hit in percent. The simulations have been done with a total of 100000 events. Events where no crystals are hit have been omitted. Bold numbers indicate the highest percentage for that energy.*

Energy	Av. cr. hit	Events in %					
E_n [MeV]	Number	1 hit	2 hits	3 hits	4 hits	5 hits	>5 hits
1	2.4	2.0	**2.8**	1.9	0.9	0.4	0.2
10	1.9	**23.1**	5.2	4.5	2.6	1.3	1.1
50	2.5	**17.9**	5.3	3.6	2.7	1.8	3.5
100	2.8	**16.4**	6.1	3.7	2.9	2.3	5.0
200	4.8	7.0	4.9	4.1	3.7	3.3	**12.4**
300	9.8	1.0	1.4	1.9	2.3	2.4	**25.9**

Table 2.5: *Number of events with two crystals hit with a space in between them. In this case a full Crystal Ball was used. The left table is for γ-rays, the table in the centre for protons and the one on the right for neutrons.*

E_γ [MeV]	Events [%]
1	0.8
2	1.1
5	2.1
10	3.2
20	4.1
30	4.3

E_p [MeV]	Events [%]
1	0.0
10	0.0
50	0.2
100	0.7
200	3.0
300	7.3

E_n [MeV]	Events [%]
1	0.6
10	1.3
50	2.4
100	4.5
200	7.7
300	7.3

Table 2.6: *The probability that the entire energy of the incident particle is deposited in the Crystal Ball. The left table shows the result γ-rays and the right for protons. The low percentage for 300 MeV protons is caused by the punch-through threshold shown in Fig. 2.3 to be around 280 MeV.*

E_γ [MeV]	Events in %
1	91.9
2	81.8
5	74.0
10	71.4
20	58.0
30	43.4

E_p [MeV]	Events in %
1	97.7
10	97.6
50	95.0
100	89.3
200	79.0
300	0.4

Table 2.7: *The tables show the probability of the first hit crystal also has the highest energy deposited. The left table is for γ-rays hitting in the middle of crystal No. 1, the middle table for γ-rays hitting at the edge of crystal No. 1 bordering to crystal No. 2 and the right table for γ-rays hitting at the corner of crystal No. 1 boarding to crystal No. 2 and 3.*

E_γ [MeV]	Events [%]
1	95.3
2	98.4
5	99.7
10	99.7
20	99.8
30	99.8

E_γ [MeV]	Events [%]
1	76.4
2	76.5
5	73.1
10	69.1
20	65.8
30	64.7

E_γ [MeV]	Events [%]
1	70.3
2	66.7
5	61.5
10	57.7
20	54.3
30	52.7

Table 2.8: *The tables show the probability of the first hit crystal has the highest energy deposited. The left table is for protons hitting in the middle of crystal No. 1 and the right table is for neutrons hitting in the middle of crystal No. 1.*

E_p [MeV]	Events in %
1	100.0
10	100.0
50	99.7
100	99.3
200	99.4
300	99.2

E_n [MeV]	Events in %
1	29.7
10	54.8
50	67.1
100	61.6
200	63.3
300	87.9

2.2 The Addback Routines

To evaluate the effectiveness of the addback routines, simulations with two guns pointing in random directions have been made. Three addback routines have been tested:

- **Neighbour**, is checking what crystal has the highest energy and add its neighbours and then checks what remaining crystal has the highest energy and add its neighbours and so on.
- **Second neighbour**, works the same way as neighbour but not only adds the neighbours but also their neighbours, i.e. the next neighbours.
- **Bunch**, also finds the crystal with the highest energy but adds all crystals with energy that is connected to it via other crystals with energy. So the routine searches for neighbours with energies, when those are found it checks if those have neighbours with energies and so on until no more crystals with energies can be found. When all crystals have been added, the crystal with highest energy among the remaining is found and the same procedure is followed for this.

An example of how the different addback routines work is shown in Fig. 2.5. Some tests were done where the bunch routine was limited to only add the three closest neighbours to ensure it does not go out of control, i.e. adding crystals all around the Crystal Ball because they are all connected. It did however not make any difference to the unlimited test and that is why the unlimited has been used throughout the simulations.

To compare the different routines it was investigated how often each routine returned the same energy as the incoming particles and how often it overestimated any of the incident energies. It is not enough to get the right total energy but it has to be right for both incident energies. For γ-rays the result is shown in Tab. 2.9 and Fig. 2.6, and for protons in Tab. 2.10 and Fig. 2.7.

The reason for the low number of overestimations for neutrons and 300 MeV protons is the definition of overestimation in the simulation. To be considered an overestimation at least one of the two summed energies has to be higher than the energy of the incident particle. Since most of the neutrons and 300 MeV protons do not deposit all their energy it is not very likely that any of the added energies are sufficiently high to cause an overestimation.

To see the separation capability of the different routines i.e. how close the hits from different γ-rays can be and still be identified as two separate hits, some

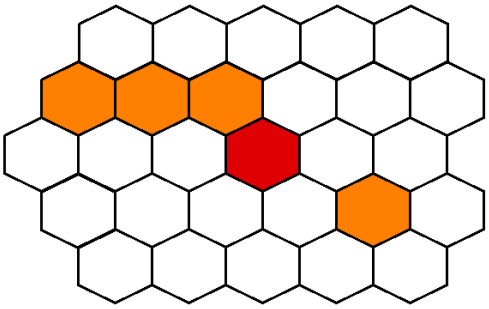

(a) Crystals with energy deposited.

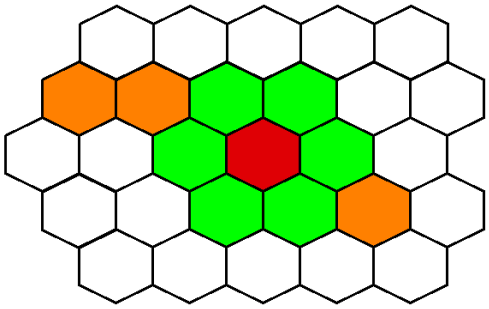

(b) Crystals added in the neighbour routine.

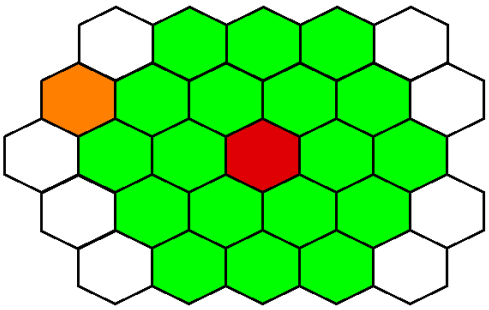

(c) Crystals added in the second neighbour routine.

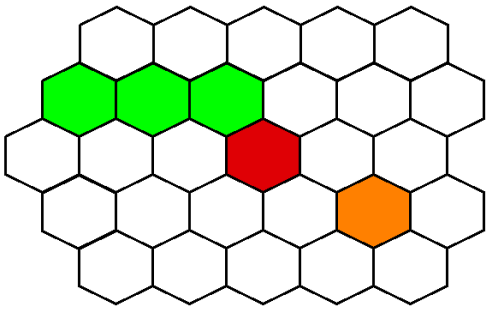

(d) Crystals added in the bunch routine.

Figure 2.5: *Fig. a shows a scenario where the incoming particle has hit the red crystal. Energies originating from the same particle has also been deposited in the orange crystals. The other three figures shows which crystals would be added for the different addback routines in this case assuming that the first hit crystal has the highest energy deposited. The crystals added to the first hit are marked with green.*

simulations were made with one fixed gun at crystal one and one sweeping from the top (crystal No. 86) down to crystal No. 1. They had the energies 5 and 10 MeV. From Tab. 2.11 it is seen that for the neighbour routine the limit is about 30°, for second neighbour about 45° and for bunch about 35° even if it starts loose some accuracy a bit earlier.

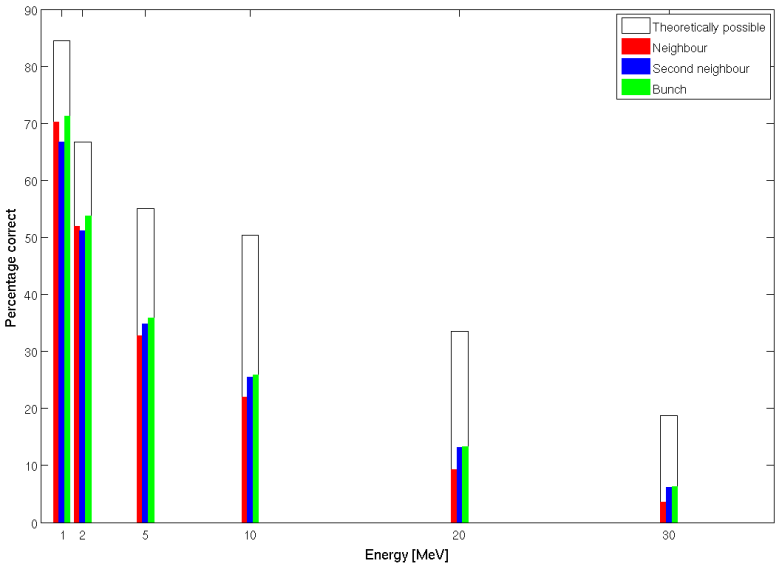

Figure 2.6: *How often the different addback routines are correct when two gamma-particles are shot at random directions in the Crystal Ball for different energies.*

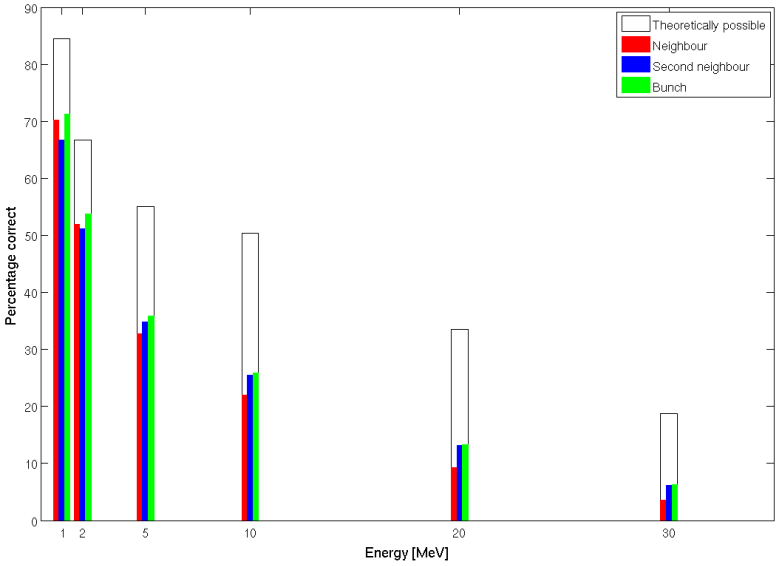

Figure 2.7: *How often the different addback routines are correct when two protons are shot at random directions in the Crystal Ball for different energies. The result for 300 MeV protons are not visible because the protons are not stopped in the crystal, thus is not the entire energy deposited in the Crystal Ball.*

Table 2.9: *The probabilities the different routines adds up the energies to the same energy as the incident γ-rays. The "Det right" column tells the probability the entire energy of the γ-rays are deposited in the Crystal Ball. Since it happens that the two γ-rays hit the same crystal it is not always even theoretically possible to detect the correct energy for the addback routine. The "Prob max" row shows the probability the routine statistically can be right. The statistical overestimations are under the assumption that no scattering has occurred. The bold numbers are the highest for those energies.*

Energies [MeV]	Det right	Overestimations in %			Correct in %		
E_1-E_2	%	Neighbour	2:nd neighbour	Bunch	Neighbour	2:nd neighbour	Bunch
Prob max	*96.3*	*4.2*	*11.5*	*4.2*	*92.1*	*84.8*	*92.1*
1-1	84.5	5.7	13.5	6.1	70.2	66.7	**71.3**
2-2	66.7	5.1	12.4	5.7	51.9	51.1	**53.8**
5-5	55.1	5.5	13.1	6.8	32.8	34.8	**35.8**
10-10	50.4	6.9	15.6	9.4	22.0	25.5	**25.9**
20-20	33.5	7.6	17.1	12.2	9.3	13.1	**13.3**
30-30	18.7	7.5	17.1	13.6	3.6	6.2	**6.3**
- - - - -	- - - -	- - - -	- - - -	- - - -	- - - -	- - - -	- - - -
10-20	41.0	6.5	14.7	10.6	14.5	**18.6**	18.5
5-10	52.7	5.7	13.2	8.2	27.0	30.2	**30.3**
1-5	68.0	4.8	11.4	6.6	48.2	48.6	**50.1**
1-30	40.0	5.2	10.0	6.7	16.1	21.1	**21.3**

Table 2.10: *The probabilities the different routines adds up the energies to the same energy as the incident protons. The "Det right" column tells the probability the entire energy of the protons are deposited in the Crystal Ball. Since it happens that the two protons hit the same crystal it is not always even theoretically possible to detect the correct energy for the addback routine. The "Prob max" row shows the probability the routine statistically can be right. The statistical overestimations are under the assumption that no scattering has occurred. The bold numbers are the highest for those energies.*

Energies [MeV]	Det right	Overestimations in %			Correct in %		
E_1-E_2	%	Neighbour	2:nd neighbour	Bunch	Neighbour	2:nd neighbour	Bunch
Prob max	*96.3*	*4.2*	*11.5*	*4.2*	*92.1*	*84.8*	*92.1*
10-10	95.2	4.1	10.6	4.1	**91.2**	84.6	**91.2**
50-50	90.4	4.3	11.2	4.3	**86.5**	80.1	**86.5**
100-100	79.7	4.9	12.3	4.9	**76.1**	70.4	**76.1**
200-200	62.7	6.3	14.7	6.5	**59.8**	55.2	59.7
300-300	0.0	3.9	9.9	5.6	**0.0**	**0.0**	**0.0**
- - - - -	- - - -	- - - -	- - - -	- - - -	- - - -	- - - -	- - - -
100-200	70.7	4.3	11.1	4.7	**67.6**	62.5	67.4
100-300	0.4	4.2	10.1	4.5	**0.4**	**0.4**	**0.4**

Table 2.11: *Percentage of times from 100000 events the different routines return the correct result when shooting two γ-rays with 5 and 10 MeV with different angular separation. The best result for each angular separation is marked in bold.*

Angular separation [deg]	Neighbour	2:nd neighbour	Bunch
90	31.7	**37.7**	35.8
80	31.3	**37.5**	35.7
70	31.3	**37.5**	35.8
60	32.1	**37.5**	36.1
50	31.0	33.1	**34.0**
45	31.4	24.6	**32.5**
40	**30.9**	11.8	29.5
35	**29.6**	1.0	26.0
30	**25.4**	0.1	21.6
25	**14.1**	0.0	11.7
20	**3.1**	0.0	2.7
15	0.0	0.0	0.0
10	0.0	0.0	0.0

2.3 Reconstruction Quality

One can also think of the possibility to only use events that fulfil certain conditions. The disadvantage is that events are discriminated, thus decreasing the statistical basis. On the other hand is the quality of the remaining events increased. Examples of possibilities are to only use events where only one crystal is added in the addback routine or there have to be back-scattered γ-rays etc. If conditions are constraining the number of crystals that are included in the addback, henceforth referred to as $\mathcal{N}$, the results in Tab. 2.12 are obtained. The results improve for lower energies with $\mathcal{N}$ equal two or three while the improvement for higher energies are negligible compared to the addback routine without conditions.

As mentioned in Sec. 2.1, a clear trace of back-scattered γ-rays at low energies can be seen. To decide if a back-scattering has occurred, the routine first makes its regular calculations. If any crystal has not been added, its energy and angle compared to the crystal with the highest energy is evaluated. If these fit in the formula for the Compton scattering also this energy is added to the total. For single γ-rays this works very well. For 1 MeV γ-rays the energies which have been "Compton corrected" are right in 99 % of all events. However, for two γ-rays with energies 1 MeV the result drops to only 40 %.

Table 2.12: *Percentage right for the three routines with $\mathcal{N}$= 1, 2 and 3. The γ-rays are shot in random directions. $\mathcal{N}$= - is the addback routine without condition for comparison.*

E_γ	Det right	Neighbour $\mathcal{N}$				2:nd neighbour $\mathcal{N}$				Bunch $\mathcal{N}$			
MeV	%	-	1	2	3	-	1	2	3	-	1	2	3
1	91.9	86.4	88.1	93.1	94.9	88.1	89.4	95.4	96.7	87.2	88.1	95.4	97.3
2	81.8	74.1	75.7	85.0	88.0	77.0	77.6	89.1	92.2	75.7	75.7	88.9	92.5
5	74.0	58.8	57.5	70.3	74.2	63.6	60.1	76.6	81.3	61.9	57.5	75.3	82.0
10	71.5	49.0	46.4	56.1	57.6	55.5	49.9	63.5	66.5	53.8	46.4	61.5	66.5
20	58.1	31.9	27.9	34.0	35.7	40.0	31.4	41.3	45.5	38.9	27.9	39.1	45.0
30	43.5	19.7	14.3	20.1	21.3	27.3	16.3	25.9	29.5	26.9	14.3	24.1	28.8

Another thing that has been investigated is the possibility to use the 511 keV annihilation photons from pair production[8]. If one searches for crystals with 511 keV deposited and assumes that its energy has to originate from pair production in its neighbour, how often does this result in the right energy? This is shown in Tab. 2.13 where a search for 511 keV energies was done and if such an energy was found, its neighbours were added to it. From the table it is obvious that this, in contrast to the condition on the number of crystals involved, works best for higher energies.

[8]When a positron is annihilated two γ-rays are created, each with an energy of 511 keV.[3]

Table 2.13: *Percentage of times the correct energy is obtained when a 511 keV crystal is found. The events with 511 keV depositions for 1 MeV γ-rays do not origin from pair production. The minimum energy needed for pair production is $2 \cdot 511$ keV, but these events in these cases are only random coincidences.*

E_γ [MeV]	Events	Correct in %
1	108	54.6
2	2878	51.1
5	14362	51.2
10	21031	54.9
20	23304	60.6
30	23652	62.9

2.4 Outlook

In these simulations three crystals have been removed (77, 81 and 82), this is where the beam pipe and the support of the target is. This is not considered in the addback routines but could affect the results. One could redefine the neighbour list, making the crystals next to the removed crystals regard each other as neighbours. This would give them eight neighbours instead of their usual six and prevent γ-rays from escaping through this gap.

It would also be interesting to investigate how the addback routines can handle background contributions and threshold energies for the crystals. Another thing to look into is the resolution as a function of the energy from real Crystal Ball data. Finally it would be interesting to find out how the resolution is affected if the energy is spread out over different crystals.

3 Position Dependence of Energy Signals in Scintillator Bars

As mentioned in Sec. 1.2.2, the LAND detector consists of 200 plastic scintillators, each equipped with two PMTs. The light intensity detected by each PMT is proportional to the energy deposited in the scintillator. However, light is attenuated in scintillators according to Eq. 1.1. Thus the energy measured by the PMTs may be written as

$$E_1 = E_0 \cdot \exp\left(-\frac{L+x}{\mathrm{f}(\lambda)}\right), \tag{3.1a}$$

$$E_2 = E_0 \cdot \exp\left(-\frac{L-x}{\mathrm{f}(\lambda)}\right), \tag{3.1b}$$

where E_1 and E_2 are the measured energies for the two PMTs, E_0 is the energy deposited in the scintillator, x is the position of the incident particle hitting the scintillator (with position zero in the middle of the paddle), $\mathrm{f}(\lambda)$ is the wavelength dependent light attenuation length, and L is half of the length of the scintillator which for LAND is 1 m.

3.1 The Smiley Effect

For physical use, it is not what the PMT itself has measured that is interesting, but rather how much energy the ion deposited. To find that, it is necessary to compensate for the losses in the scintillator. If the Eqs. 3.1a and 3.1b are multiplied with each other and then taken the square root of, the result obtained is

$$\sqrt{E_1 E_2} = E_0 \cdot \exp\left(-\frac{\mathrm{L}}{\mathrm{f}(\lambda)}\right).$$

Since E_0, L and $\mathrm{f}(\lambda)$ all are independent of the hit position x, it is clear that also $\sqrt{E_1 E_2}$ should be independent of the hit position of the hit in the scintillator. To check this, a plot of $\sqrt{E_1 E_2}$ versus the position of the hit can be made. That is what is shown in Fig. 3.1, using data from paddle No. 12 in plane No. 5 of the LAND detector. The data were obtained during experiment S245. As can be clearly seen in the figure, the energy is not independent of the position of the

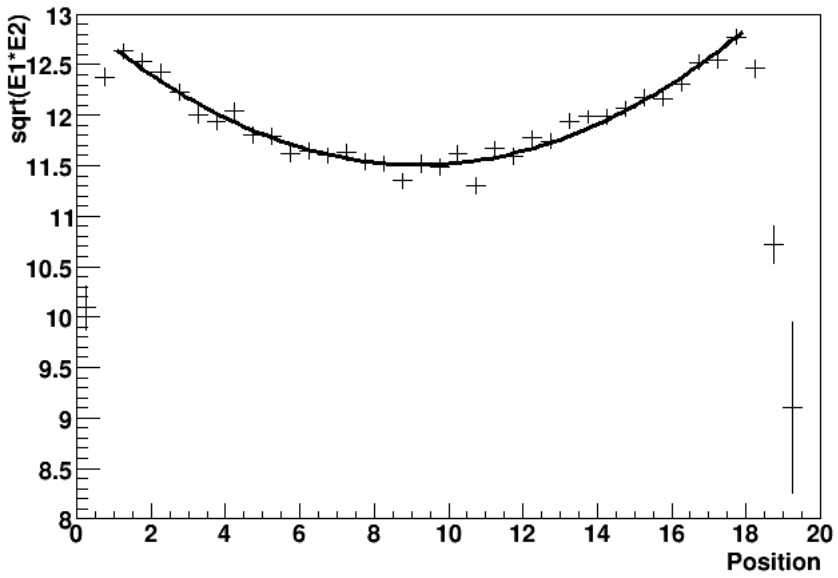

Figure 3.1: *The plot shows $\sqrt{E_1 E_2}$ in uncalibrated units versus the position of the hit expressed in paddles. The black line is a second degree polynomial fit. The data used were obtained during experiment S245 for paddle No. 12 in plane No. 5 of the LAND detector.*

hit. The key question is why the energy is changing with the position of the impact. The conclusion must be that the signal attenuation in the scintillator is not completely described by Eqs. 3.1. Another thing that is noted in the figure is the behaviour at the far edges of the scintillator. Instead of increasing further, the energy drops drastically.

3.2 Energy Loss in Scintillators

Several factors might affect the energy loss in the scintillator. One important factor is the reflections at the scintillator surface. Assuming that the light created by an incoming particle can be approximated as a point source of light, the fraction of the light hitting the PMTs depends on the position of this point source. Depending on geometry, only a small fraction of the total light reach the PMTs directly. Because the length of the scintillator is much larger than the width, most of the light is reflected many times at the surface of the scintillator on its way to the PMTs. Depending on the angle of the light hitting the surface there are some losses. The path length of light increases with the number of reflections and thereby the light attenuation. Another important factor is the possibility that light reaching PMT1

is reflected at the surface of the photo cathode towards PMT2 or vice versa, thus creating an erroneous relation between the two measured energies [13].

To compensate for the additional signal loss of the energy measurement, Eqs. 3.1 are multiplied with a reflection factor for the surface and another for the PMTs. In addition the attenuation loss factor is modified, resulting in Eqs. 3.2 [14].

$$E_1 = E_0 \left((1-\alpha) \exp\left(-\frac{4(L+x)}{\mathrm{f}(\lambda)(1+\cos\gamma)^2} \right) \cdot \mathrm{R}(L+x,\rho,\gamma) + \alpha \cdot \exp\left(-\frac{4(3L-x)}{\mathrm{f}(\lambda)(1+\cos\gamma)^2} \right) \cdot \mathrm{R}(3L-x,\rho,\gamma) \right), \tag{3.2a}$$

$$E_2 = E_0 \left((1-\alpha) \exp\left(-\frac{4(L-x)}{\mathrm{f}(\lambda)(1+\cos\gamma)^2} \right) \cdot \mathrm{R}(L-x,\rho,\gamma) + \alpha \cdot \exp\left(-\frac{4(3L+x)}{\mathrm{f}(\lambda)(1+\cos\gamma)^2} \right) \cdot \mathrm{R}(3L+x,\rho,\gamma) \right). \tag{3.2b}$$

The first exponential term is an average of the possible pathway simply taking $x \cdot (\frac{\cos(0)+\cos(\gamma)}{2})^{-1}$ where γ is the critical angle at the PMT. Since the reflections can occur in two dimensions (the width of the paddle, and the height of the paddle), the total is given by the square i.e. $x \cdot (\frac{(1+\cos(\gamma))^2}{4})^{-1}$ which is the average path length for a photon in the scintillator reaching a PMT. The second exponential term originates from the reflection at the opposite PMT with the reflection fraction α. The function R describes the loss due to reflections at the surface of the scintillator. This is only calculated in one dimension due to the fact that the scintillators are much higher than they are thick, thus are the reflections in the height dimension neglected. For scintillators with more equally sized height and thickness each term have to be multiplied with another R function replacing the thickness d in Eq. 3.3 with the height of the paddle. The function R is described by a sum as,

$$\mathrm{R}(x,\rho,\gamma) = \sum_{i=0}^{\frac{x\tan(\gamma)}{d}} \frac{\rho^i \cdot (\theta_{i+1} - \theta_i)}{\frac{\pi}{2}} \tag{3.3}$$

Here ρ is the reflection coefficient at the surface, and γ is the critical angle for total reflection between the scintillator and the PMT. The angle $\theta_i = \mathrm{atan}\left(\frac{d \cdot i}{x}\right)$ is the minimum angle needed for i number of reflections before hitting the PMT.

Even though it is hard to know the exact values for the constants in Eqs. 3.2 and 3.3, some reasonable values could be $\mathrm{f}(\lambda) \approx 180$ cm, $\gamma = 58°$, $\rho = 0.985$ and $\alpha = 0.25$. In Fig. 3.2 is the plot of $\sqrt{E_1 E_2}$ shown for a LAND scintillator using these values. Multiplying with a constant, this function agrees well with the one in Fig. 3.1.

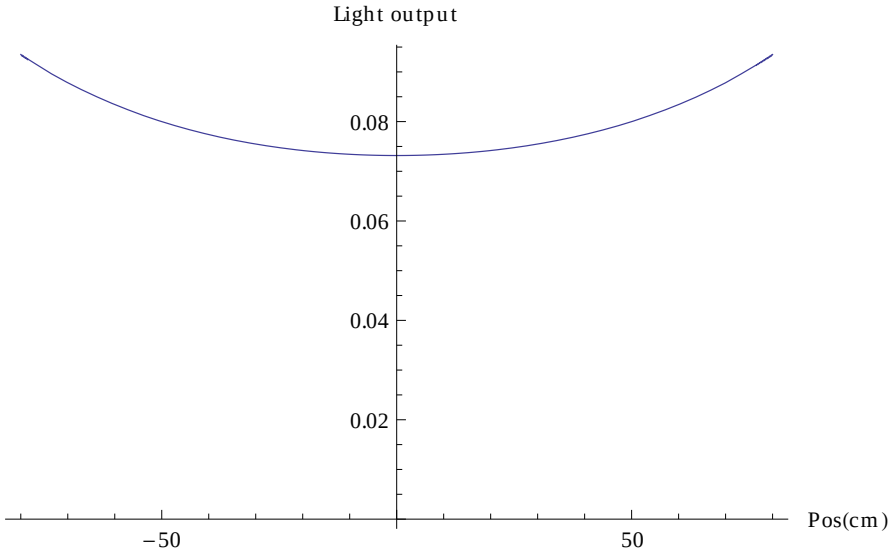

Figure 3.2: *The function* $\sqrt{E_1 E_2}$ *for a LAND scintillator bar when using values* $f(\lambda) \approx 180$ *cm,* $\gamma = 58°$*,* $\rho = 0.985$ *and* $\alpha = 0.25$*.*

3.3 Compensating the Losses

Even though Eqs. 3.2 describes the losses in the scintillators in a physical way it is not an easily applicable correction because the equations are quite complex and the constants are hard to determine for each paddle. A more accessible correction is based on a second degree polynomial with the hit position as variable. For LAND the parameters can be obtained by a fit to data obtained from detecting cosmic muons, see Fig. 3.1. For other detectors such as the TFW and NTF it is a bit more tricky. Since the TFW and NTF have only two planes each, it is not possible to calculate the trajectory of a muon hitting. Without knowing the trajectory it is not possible to know the distance travelled in the scintillator and thereby the actual deposited energy. Instead other methods have been considered. The method that has worked best is a method where the energy spectrum of different ions is used. Other methods which have been used, or at least have been tried, are an internal correction between the paddles and a method using a data fitting tool. These two methods along with the muon method are discussed in appendix A.

3.3.1 Using Ions for Correction

The method which has showed the best results is using the energy spectra obtained for different ions. The basic idea is that the spectra should look similar independent

of the hit position in the paddle. A paddle of the NTF detector, with 8+8 paddles, can be divided into eight sections based on the other plane of scintillators. By plotting the energy spectrum for one section of a paddle at a time, the change in the spectra can be seen. This is caused by the smiley effect, but if this can be corrected for, it means that also the smiley effect is corrected for. The biggest problem with this method is that the ions hitting the TFW and NTF are quite centred in the middle of the detectors as shown in the hit pattern in Fig. 3.3. The lack of data at the ends of the paddles makes a correction harder to find since it is at the ends the effect of the smiley is most significant. There are several different ions in the beam and the different ions deposit different amounts of energy in the scintillators. In order to be able to find the smiley effect one has to be able to distinguish between the different ions in the data. The deposited energy in the scintillators of the ions can be calculated with the Bethe-Bloch formula [3].

$$-\frac{\mathrm{d}E}{\mathrm{d}x} = 2\pi N_\mathrm{a} r_\mathrm{e}^2 m_\mathrm{e} c^2 \rho \frac{Z}{A}\frac{z^2}{\beta^2}\left(\ln\left(\frac{2m_\mathrm{e}\gamma^2\beta^2c^2W_\mathrm{max}}{I^2}\right) - 2\beta^2 - \delta - 2\frac{C}{Z}\right). \quad (3.4)$$

Here N_a is Avogrado's number, r_e the electron radius, m_e the electron mass, ρ the density of the material, Z the number of protons in the material, A the number of nucleons in the material, z the charge of the particle in e, β speed of the incident particle in c, γ the Lorentz factor, W_max the maximum energy transfer in a collision, I the mean excitation potential, δ is a density correction and C is a shell correction. Most of the terms in the equation are identical for all the ions because they traverse the same medium. A reasonable approximation in this case would be that

$$-\frac{\mathrm{d}E}{\mathrm{d}x} \propto \frac{z^2}{\beta^2}. \quad (3.5)$$

Another simplification which can be made in this case is the assumption that all the ions have the same velocity. The ions will have a minor difference in their speed but the major difference in their energy deposition is caused by their charge.

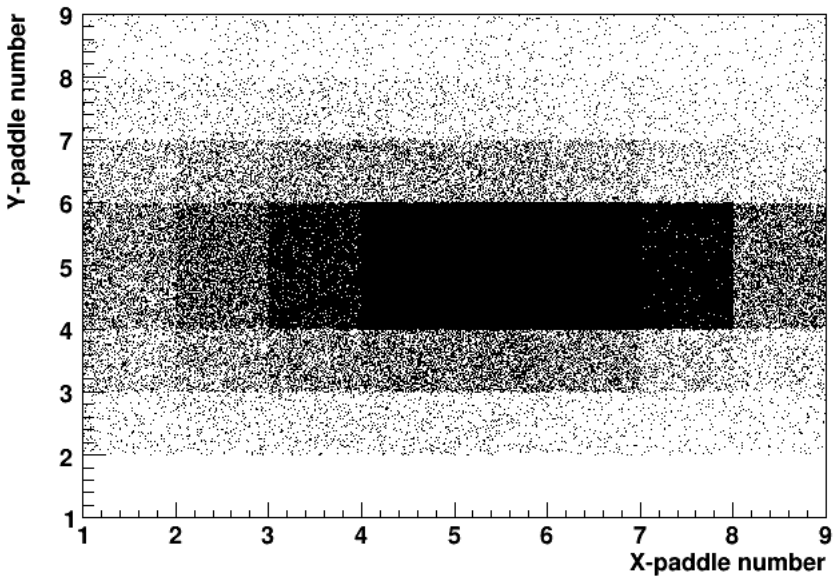

Figure 3.3: *The hit pattern for the NTF from experiment S327. A dot between 2 and 3 correspond to a hit somewhere in paddle No. 2, a dot between 3 and 4 correspond to a hit somewhere in paddle No. 3 and so on. Paddle No. 1 in the y-plane did not work properly during the experiment.*

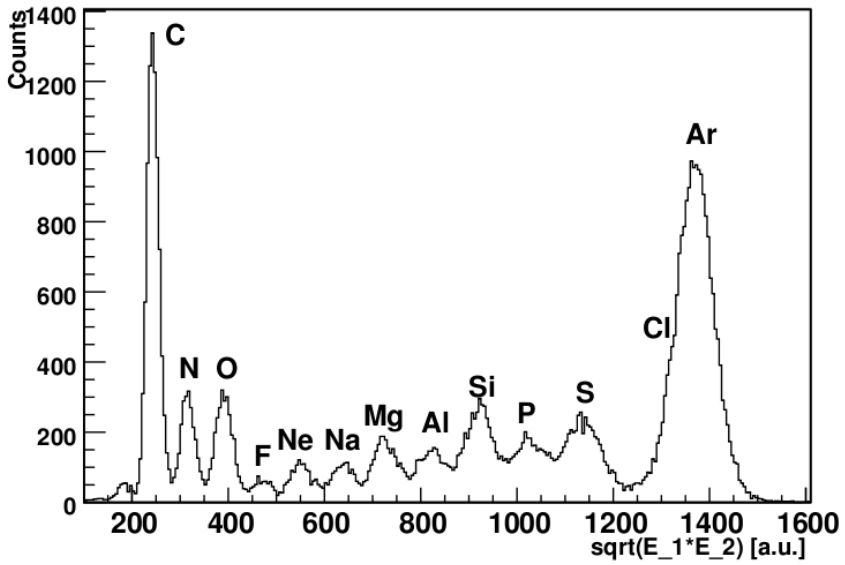

Figure 3.4: *The energy spectrum for paddle No. 4 in the y-plane at the intersection with paddle No. 3 in the x-plane. Each peak correspond to one ion species. Data taken from experiment S327.*

According to Eq. 3.5, ions with a higher z will deposit more energy in the scintillators than those with a lower z if they have approximately the same velocity. In Fig. 3.4 the energy spectrum is plotted for paddle No. 4 in the y-plane at the intersection with paddle No. 3 in the x-plane of the NTF. In this figure there are clear peaks corresponding to different ion species. The beam in this experiment was ^{32}Ar which has $z = 18$. Since no fusion reactions occur during the experiment the peak with the largest energy loss in the spectrum indicates the unreacted beam consisting of Ar. This peak is quite broad, obscuring the peak for Cl. The peak for Cl is visible at other positions in the paddle though. Thereafter follow the different ions with decreasing z down to C.

Using the same plot as in Fig. 3.4 at the different intersections of the paddle, taking the peak positions for each ion, and plotting this against the position, the smiley effect should become visible. However, as mentioned before and demonstrated in Fig. 3.3 the statistics is not very good near the ends of the paddles. This can be seen in Fig. 3.5 for paddle No. 4 in the y-plane which has the most statistics at the ends. In this case the peaks for $z = 6$, 7 and 8 are difficult to identify.

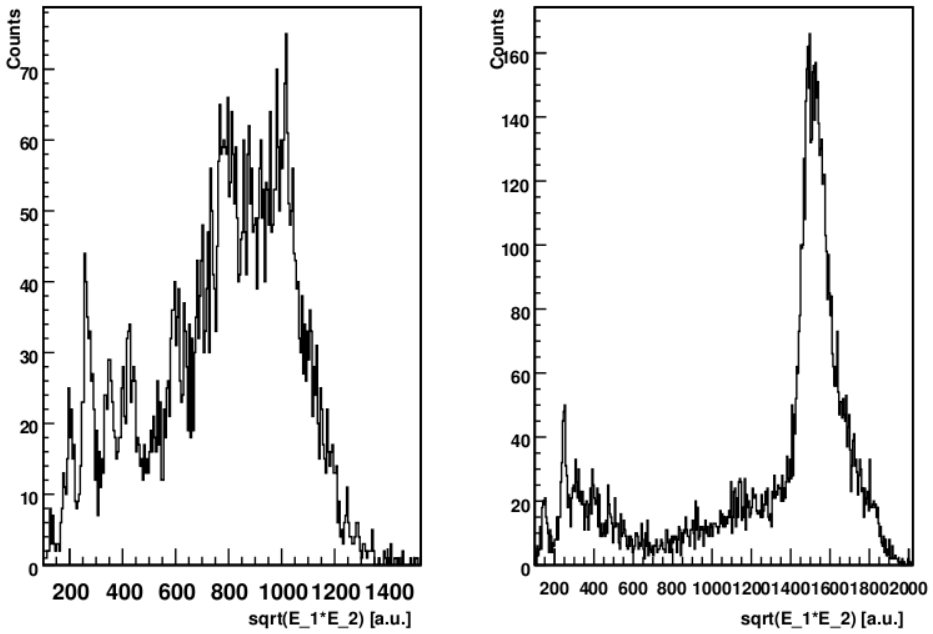

Figure 3.5: *The energy spectrum for paddle No. 4 in the y-plane at the intersection with paddle No. 1 to the left and No. 8 to the right in the x-plane. The data is taken from experiment S327.*

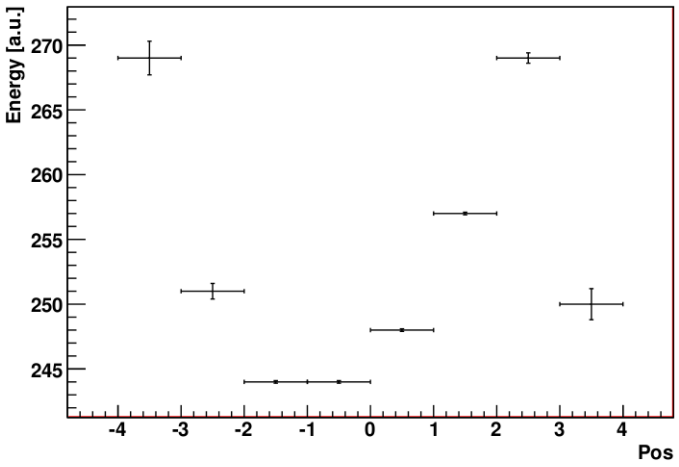

Figure 3.6: *The energy in paddle No. 4 of the y-plane in the NTF-detector plotted against the hit position in the paddle, i.e. what intersection the ion passed. For this plot the carbon ions have been used.*

If the peaks at $z = 6$ are chosen at each position, and a Gaussian fit is applied, the smiley can be plotted as in Fig. 3.6. The error bars in y are given by the error estimation of the peak position given by the Gaussian fit and the error in x is given by the resolution of the position i.e. the paddle width. An interesting feature which has been recognised in both the LAND-, TFW- and NTF-data is the decreasing energy at the ends of the scintillators. This can be seen in both Fig. 3.1 and 3.6. This feature has not been thoroughly investigated but is ignored throughout this thesis. A second degree polynomial fit to the graph in Fig. 3.6 results in the equation

$$\begin{aligned} E_{\text{meas}} &= \mathrm{p}_0 + \mathrm{p}_1 x + \mathrm{p}_2 x^2 \\ \mathrm{p}_0 &= 245 \pm 0.1 \\ \mathrm{p}_1 &= 4.19 \pm 0.04 \\ \mathrm{p}_2 &= 2.34 \pm 0.04, \end{aligned} \tag{3.6}$$

where x is the position given in paddle widths with zero representing the middle of the paddle. Due to the lack of statistics at the end of the paddle and the fact that not all ions hit all the positions of the paddle this fit is difficult to perform for all ions. The ions with the most distinct peaks at all the positions from -4 to 3 are z =6, 7, 8, 10, 12 and 14. Fitting those peaks, as described above for $z = 6$, results in the coefficients of the second degree polynomial for each ion species. The values obtained are given in Tab. 3.1.

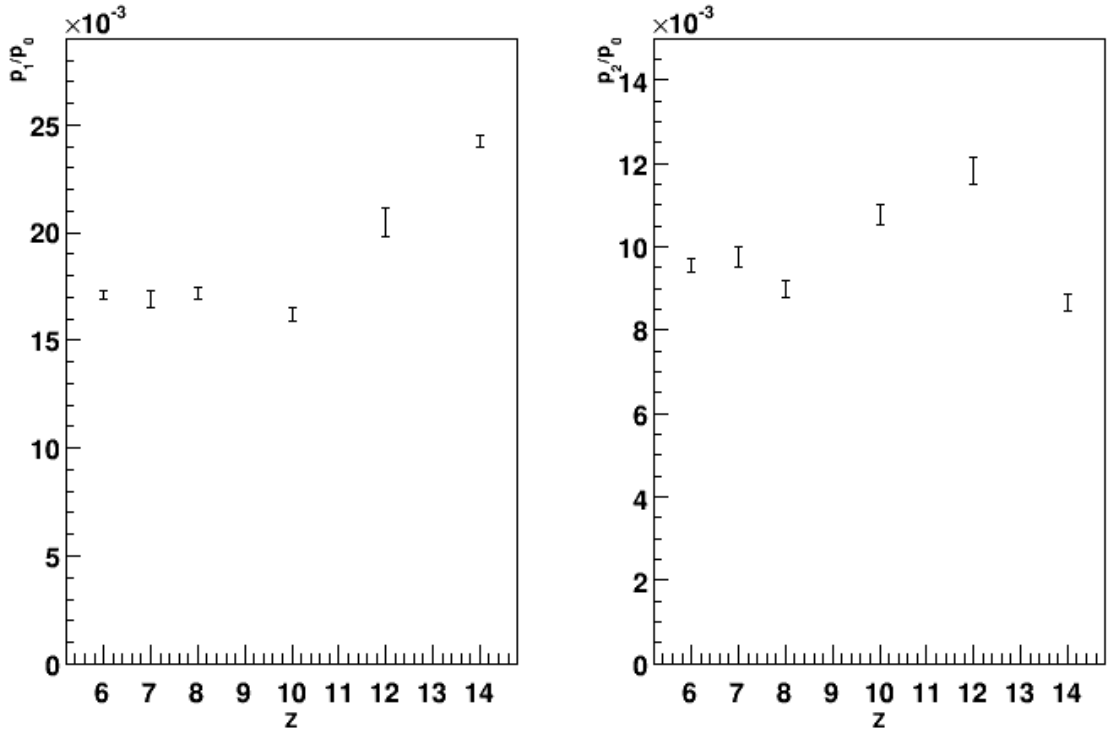

Figure 3.7: *The coefficients* $\frac{p_1}{p_0}$ *and* $\frac{p_2}{p_0}$ *for different ions. As can be seen, both* $\frac{p_1}{p_0}$ *and* $\frac{p_2}{p_0}$ *are almost the same for different z.*

Table 3.1: *The coefficients for the smiley correction for different nuclear charge numbers. The coefficients* $p_{10} = \frac{p_1}{p_0}$ *and* $p_{20} = \frac{p_2}{p_0}$.

z	p_0	p_1	p_2	$p_{10} \cdot 10^2$	$p_{20} \cdot 10^2$
6	245 ± 0.1	4.19 ± 0.04	2.34 ± 0.04	1.71 ± 0.09	0.95 ± 0.06
7	318 ± 0.1	5.39 ± 0.12	3.11 ± 0.08	1.69 ± 0.04	0.98 ± 0.02
8	394 ± 0.1	6.76 ± 0.11	3.55 ± 0.08	1.72 ± 0.03	0.90 ± 0.02
10	554 ± 0.4	8.98 ± 0.18	5.97 ± 0.13	1.62 ± 0.03	1.08 ± 0.02
12	732 ± 0.7	15.0 ± 0.49	8.67 ± 0.24	2.05 ± 0.06	1.18 ± 0.03
14	946 ± 0.6	22.9 ± 0.29	8.21 ± 0.18	2.42 ± 0.03	0.87 ± 0.02

Even though there are only six data points for each coefficient, it is obvious that they change for different ions. This is caused by the different energies deposited by ions with different nuclear charge in the detector according to Eq. 3.5. This is a problem independent of the correction method. The solution to this problem is to factor out p_0 from Eq. 3.6 and obtain the equation

$$E_{\text{meas}} = p_0 \left(1 + \frac{p_1}{p_0} x + \frac{p_2}{p_0} x^2\right). \tag{3.7}$$

The advantage of having the equation on this form is that the coefficients $\frac{p_1}{p_0}$ and $\frac{p_2}{p_0}$ do not vary with the deposited energy which can be seen in Fig. 3.7 where $\frac{p_1}{p_0}$ and $\frac{p_2}{p_0}$ are plotted against z. Even though some points differ quite much from the rest it is still reasonable to consider the coefficients to be constant. Since the two coefficients vary slightly for the different ions, the values are taken as the average of all ions giving $\frac{p_1}{p_0} = p_{10} = 1.86 \cdot 10^{-2}$ and $\frac{p_2}{p_0} = p_{20} = 0.99 \cdot 10^{-2}$. Now it is possible to apply a correction for all energies at all the positions in the scintillator. From Eq. 3.7 the coefficient p_0 can be replaced with E_0, which is assumed to be the energy deposited in the detector, i.e. the wanted energy. This provides the equation

$$E_0 = \frac{E_{\text{meas}}}{1 + p_{10} x + p_{20} x^2}. \tag{3.8}$$

To see if this correction really works it is necessary to apply the correction and compare the result with the uncorrected data. In Fig. 3.8 the original energy spectra are plotted while Fig. 3.9 presents corrected energy spectra. At lower energies the correction works very well. At higher energies it is not as good but it still improves the result significantly. The reason the spectrum for Pos 3.5 is not shown in the plots is that the correction is not valid for that position. As was shown in Fig. 3.6, the energy decreases again instead of following a second degree curve. Hence that spectrum has been neglected in the evaluation.

The result for paddle No. 4 is good. When performing the same correction procedure for paddle No. 5 as for No. 4, the coefficients obtained in the second degree polynomial is $p_{10} = 0.19 \cdot 10^{-3}$ and $p_{20} = 0.59 \cdot 10^{-2}$ which differ alot compared to those obtained for paddle No. 4. When applying the correction for paddle No. 5 though, the result of the correction is very similar to the result for paddle No. 4. This further consolidates that this correction method works. It also shows that it is necessary to obtain separate second degree polynomials coefficients for different paddles.

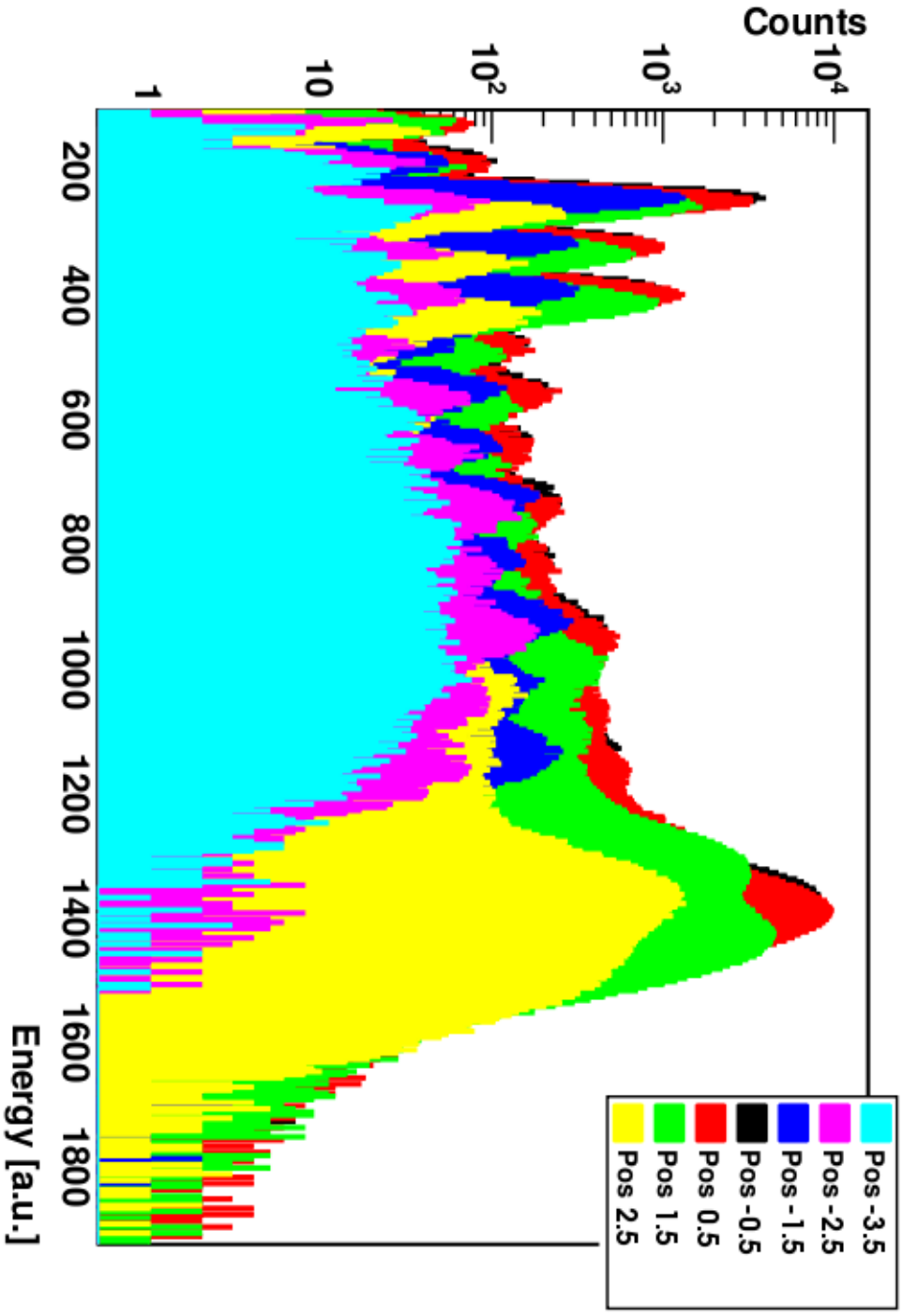

Figure 3.8: *The energy spectra for paddle No. 4 in the y-plane at different positions in the paddle before the correction has been applied. The reason the spectra do not overlap each other as wanted has the same origin as the smiley effect. By correcting the data such that the spectra overlap each other, also the smiley effect is neutralised.*

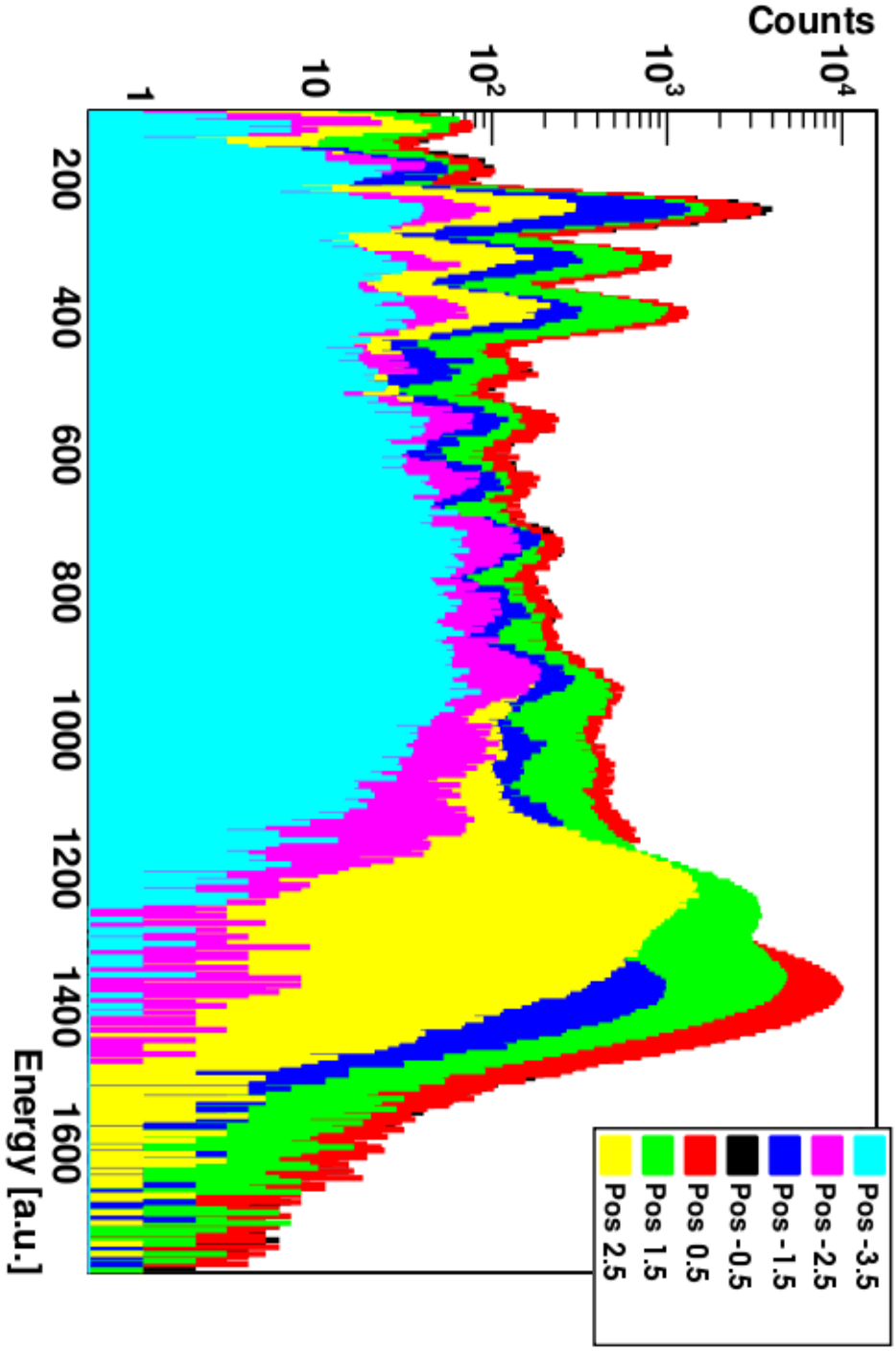

Figure 3.9: *The energy spectra for paddle No. 4 in the y-plane at different positions in the paddle after the correction has been applied. In contrast to Fig. 3.8 the spectra are overlapping each other well. This is a proof that the applied correction achieves the desired result.*

3.4 Outlook

In this chapter a method has been found to correct the smiley effect in LAND, TFW and NTF. The biggest problem of the method proposed, is that it demands high statistics also close to the PMTs. Because the beam is quite centred such data are usually not available. This is especially a problem in the x-plane because the variation in height is less than the variation in horizontal position, as can be seen in Fig. 3.3. Furthermore, the beam position cannot be altered vertically but only horizontally and also ALADIN can only bend the ions horizontally. To be able to correct all the paddles in the TFW and NTF detectors this problem needs to be solved.

Another problem is the poor position resolution. This can partly be solved by extracting the position based on the time difference between the two PMTs. This would probably improve the resolution, but it would still be a large source of error. Another solution would add two more layers of scintillators which can be used to track the path of the ion through the detector. A third solution would use the tracking detectors in front of the TFW and NTF detectors thereby reduce this uncertainty. If the threshold of the CFD[9] is decreased to be able to detect muon energies, it might be possible to use the method described in App. A.1.

Another topic that requires further investigation is the behaviour of the detectors when the ion hits close to the PMTs. As seen in Figs. 3.1 and 3.6 the deposited energy drops fast. The cause of this behaviour has not been investigated in this work. One idea is that when the hit occurs close to a PMT the light produced hit the PMT with a higher intensity and within a smaller time gap. It might be possible that the PMT is not able to detect such an intense signal but loose some of its energy, hence would the energy decrease.

[9]Constant Fraction Discriminator is an electronic module that converts an analog signal with amplitude above a certain threshold to a logic signal.

4 Muon-Proton Correlation in the Crystal Ball

To get a relation between the measurements of muon energies and proton energies as deposited in the Crystal Ball a detector system called CXB was built. This relationship will be useful to calibrate the proton branch of the Crystal Ball. Calibrating the Crystal Ball for proton energies is a challenging task, because there are no proton sources with sufficiently high energies, $\sim$ 200 MeV, which is about the energy a proton would deposit. These energies can only be achieved with an accelerator. The experiment S406 was performed to test the first NeuLAND prototype and to calibrate LAND. This was done using a deuteron beam at different energies, ranging from 200 A MeV up to 1500 A MeV. Both NeuLAND and LAND are aimed at detecting neutrons, so the deuterons are shot into a target in order to split the nucleus, creating single neutrons. One byproduct from this reaction is the remaining protons with rather well defined energies. These protons were also used during the experiment to test other detectors such as the CXB. A drawing of the most important detector systems during the experiment is shown in Fig. 4.1

4.1 CXB

The design of the CXB-detector is based on simulations performed as part of a Bachelor project [15] at Chalmers during spring 2012. The idea is that muons should pass through one scintillator, continue through the crystal and then hit another scintillator. With the information of which scintillators have been hit, the distance the muon has travelled through the crystal can be calculated. The detector consists of one crystal from the Crystal Ball and six scintillators as shown in Fig. 4.2. The scintillators are placed to cover different solid angles. Since the majority of the cosmic muons are in the minimum ionising energy range, the energy deposited in the crystal is well defined, thus being proportional to the distance travelled in the crystal. This is not the case for the protons. They will come from the front traversing the crystal and exit in the back unless the protons are stopped in the crystal or scattered at very large angles. If they are stopped in the crystal their kinetic energy is measured, but if they escape the crystal, only a part of their energy will be measured. This measured energy will vary with the energy of the incoming proton, the higher incident energy the lower measured energy.

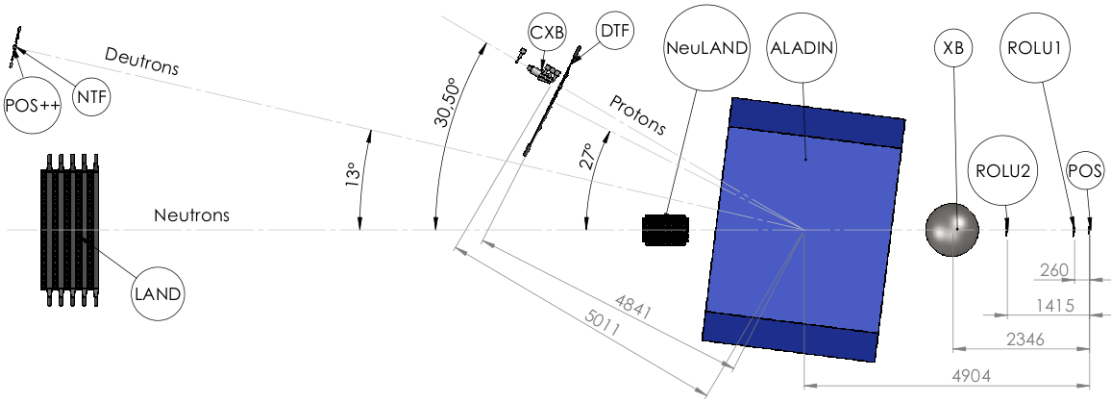

Figure 4.1: *The experimental setup during experiment S406. Not all the detectors present in the experiment are shown, but the most important ones for the experiment and for the CXB. All distances are given in mm.*

4.2 Data Analysis

What easily could be seen in the data was that the secondary proton energies, i.e. the single protons created in the target, were lower than expected. Fig. 4.3 shows the energy deposited in the crystal versus the time of flight from the start-detector (POS) to the CXB. In the figure the energy peak is found in the 400 A MeV deuteron run. The expectation was to see this punch-through limit peak in the 300 A MeV deuteron run. Since simulations place it at about 280 MeV, as shown in Fig. 2.3. The fact that this peak is present in the 400 A MeV deuteron run is thus surprising. To check the energies of the protons, the current in ALADIN can be used. Since the protons are bent differently according to their momentum it is possible to calculate the kinetic energy of the protons impinging on the CXB from its angle with respect to the incoming beam. The bending power of the magnet can be calculated as

$$B\rho = \frac{m_{\mathrm{u}}c}{e}\frac{A}{Z}\beta\gamma, \tag{4.1}$$

where B is the magnetic field, ρ the radius of curvature, m_{u} is the atomic mass unit and e the electron charge. A is the mass number of the ion, Z is the atomic number, β is the speed as $\frac{v}{c}$ and γ is the Lorentz factor $\frac{1}{\sqrt{1-\beta^2}}$. But B can be calculated from the current of the magnet using a second degree polynomial [16] and ρ can be calculated as

$$\rho = \frac{L}{2\,\sin\frac{\psi}{2}\,\cos(\alpha - \frac{\psi}{2})}. \tag{4.2}$$

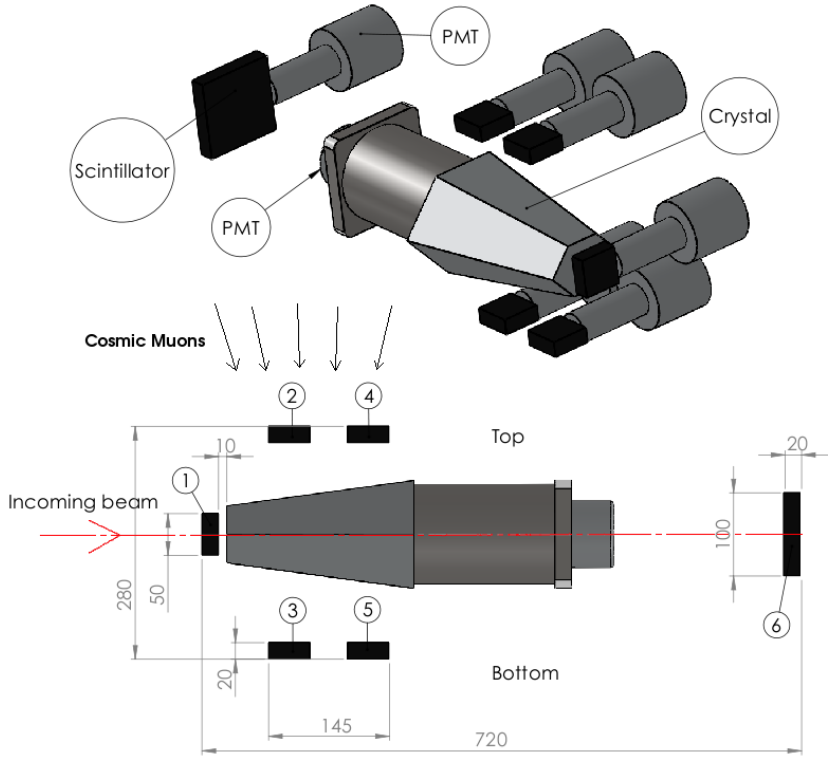

Figure 4.2: *A schematic drawing of the CXB detection system. The numbers in the lower drawing indicate the numbering of the scintillators used during the experiment. Scintillator 1 is in front and scintillator 6 in the back. All dimensions are given in mm.*

L is the effective length of the magnet, in this case 1.4 m, α is the angle between the normal to the trajectory of the incoming ion and the front of ALADIN while ψ is the angle between the outgoing ion and the trajectory of the incoming ion. By combining Eq. 4.1 and 4.2 the energy T at a certain angle can be calculated,

$$T = m_0 c^2 \left(\left(1 - \frac{1}{1 + \left(\frac{2kA \cdot \sin\frac{\psi}{2} \cos(\alpha - \frac{\psi}{2})}{(p_0 + p_1 I + p_2 I^2) LZ} \right)^2} \right)^{-\frac{1}{2}} - 1 \right), \tag{4.3}$$

where m_0 is the rest mass of the ion, $k = \frac{m_u c}{e}$ is a constant with value 3.10716 NA^{-1} and p_0=-0.13798, $p_1 = 0.11337 \cdot 10^{-2}$ and $p_2 = -0.16974 \cdot 10^{-6}$ are the second degree polynomial coefficients from Ref. [16].

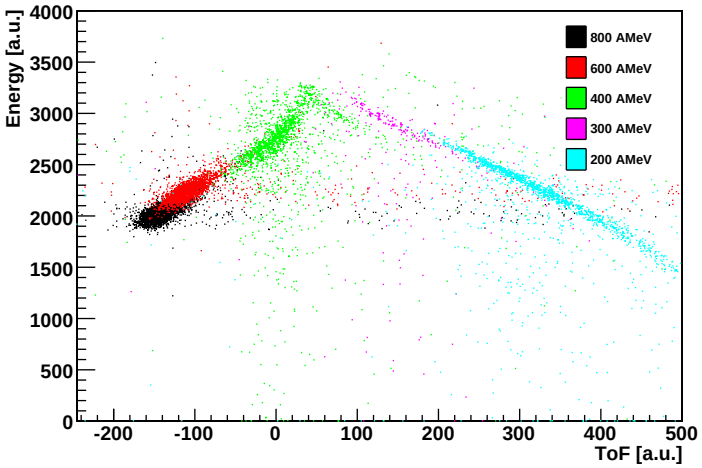

Figure 4.3: *The energy deposited in the crystal as a function of the time of flight of the protons between the POS and CXB detectors. The different colours correspond to different beam energy settings. Both axes are uncalibrated.*

4.2.1 Time Calibration

From the currents in the different runs and the knowledge of the angles $\alpha = 6.0°$ [17] and $\psi = 30.5°$ for the CXB, the energies of the protons can be calculated. These are presented in Tab. 4.1. These values correspond very well to the result in Fig. 4.3 with the punch-through limit in the 400 A MeV run. The next step is to calibrate the time of flight. The calibration of the time gain is done via a script called `tcal`. From the script the calibration parameters are obtained and it is only the offset that still needs to be shifted. That is because of different cable lengths in the setup, with longer cables it will take longer time for the stop signal to reach the TDC which is the unit measuring the time. To get the offset a deuteron sweep run with an empty target was used[10]. The ions hitting the detector are then deuterons with less energy straggling than in the target runs. With Eq. 4.3 the energy is given and from the energy the time of flight can be calculated since the distance between the POS-detector and the CXB is known to be 10.38 m. With this calibration the x-axis of Fig. 4.3 can be calibrated to get a real time scale.

[10]Sweep runs are performed without a target to get a narrow unreacted beam. The sweep is performed by slowly changing the current in ALADIN back and forth, thus sweeping the beam over a detector for example.

Table 4.1: *The run number, the incident deuteron energies and the proton energies calculated from Eq. 4.3 in the different runs. The runs r334 and r367 are deuteron sweep runs. The current values given are the calculated value for deuterons hitting the centre of the detector and the values within parenthesis is the range of the sweep. The energy values for the sweep runs are calculated from the current as for the protons but using the deuteron mass.*

Run	T_d [A MeV]	I [A]	$T_{p/d}$ [MeV]	Note
r258	300	973	205	proton
r323	800	2190	620	proton
r328	200	780	136	proton
r334	200	2028 (1850–2150)	344	deuteron sweep run
r352	600	1605	441	proton
r361	400	1194	289	proton
r367	100	1109 (770–1325)	140	deuteron sweep run

4.2.2 Muon Calibration

To calibrate the energy, cosmic muons are used. As mentioned earlier these are minimum ionising and hence have a well defined energy deposition. By looking at the data and using coincidences between the different scintillators surrounding it, the transformation factor to MeVs is obtained. The path length in the crystal for different scintillator combinations are presented in Tab. 4.2. To check if the

Table 4.2: *The path length in the crystal depending on which plastic scintillators have been hit in coincidence.*

Scintillators	Path length [cm]
2 & 3	8.9 ± 0.7
4 & 5	11.5 ± 0.7
1 & 6	20.0 ± 0.1

data agree with the assumption that the energy deposited only is dependent on the travelled path length in the crystal, one can check if the fraction between the path lengths are the same as the fraction between the peak values in Fig. 4.4. They prove to agree well according to Tab. 4.3. From the simulations in Ref. [15] the deposited energy is approximately 105 MeV for muons travelling 20 cm in the crystal, giving the calibration factor. With both the time and energy calibration applied, Fig. 4.5 is obtained. From the time of flight the energy of the proton can

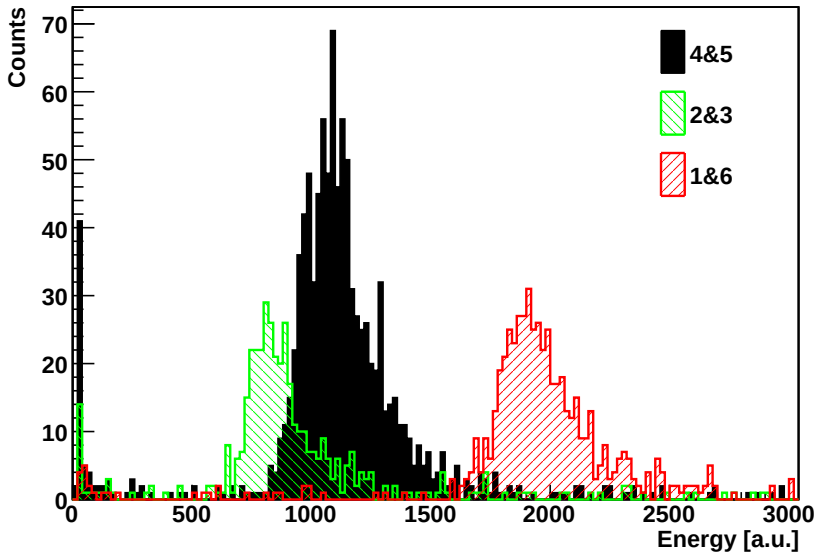

Figure 4.4: *The energy deposited in the crystal by cosmic muons with different path lengths through the crystal. The legend tells which scintillator pairs have coincident hits for each colour.*

Table 4.3: *The fractions of the path lengths and the peak positions in Fig. 4.4. The numbers in the first column indicate the scintillators which were hit, see text.*

Fractions	Path lengths	Peak positions
$\frac{2\&3}{4\&5}$	0.77	0.77
$\frac{2\&3}{1\&6}$	0.44	0.43
$\frac{4\&5}{1\&6}$	0.57	0.55

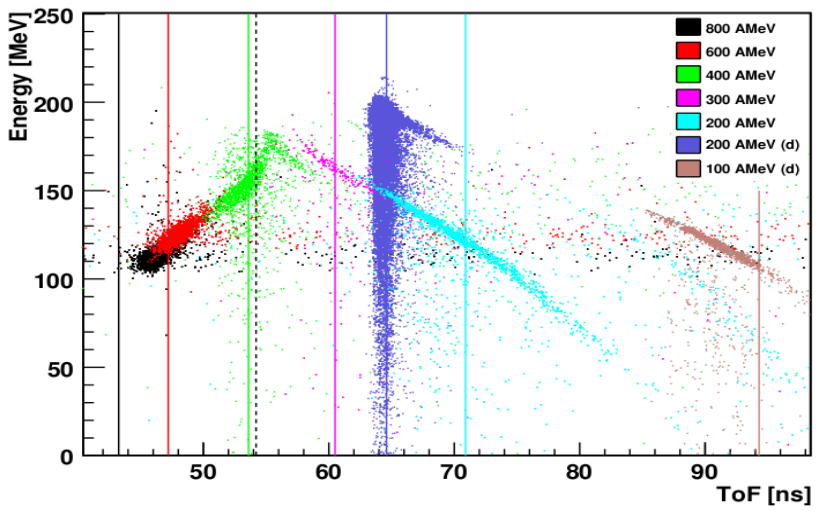

Figure 4.5: *The energy deposited by protons/deuterons in the CXB crystal plotted against time of flight from the start detector (POS) to the CXB. Vertical lines mark the expected time of flight for the related run and the dashed line is the expected time of flight for the punch-through limit. The two runs marked with (d) in the legend are sweep runs with deuterons. The 200 A MeV deuteron sweep run has been used for offset calibration, using the energy value derived from the magnet current.*

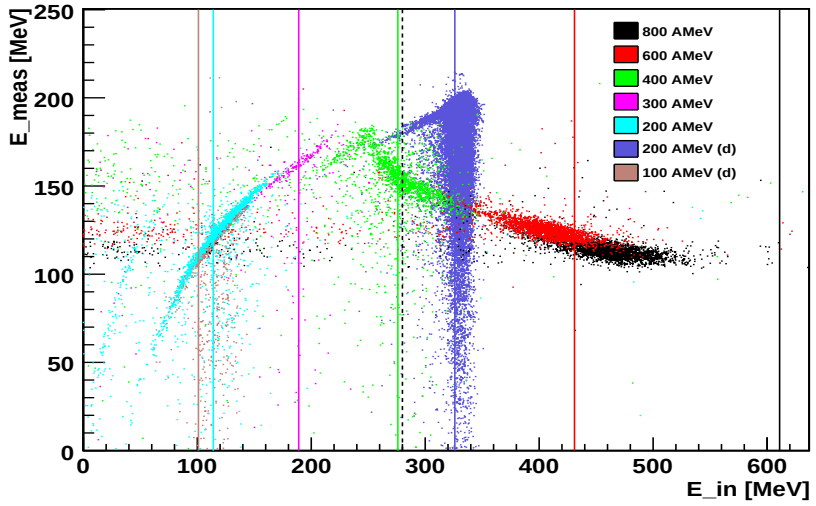

Figure 4.6: *The measured energy versus the incoming kinetic energy calculated from the time of flight, see Fig. 4.5 and corrected for the energy loss in the plastic scintillators, see text. The vertical lines are the expected energy in that run and the dashed line is the expected punch-through energy.*

also be calculated. This energy has to be corrected though. This is because of the two plastic scintillation detectors in front of the crystal. First the DTF detector and then plastic scintillator No. 1 in the CXB detector. Since these two detectors are placed very close to the crystal (<30 cm) they do not affect the time of flight but only the energy of the particles hitting the crystal. The two detectors together adds 3.5 cm of plastic for the particles to traverse before impinging on the crystal. The energy loss in 3.5 cm of plastic has been simulated using ATIMA [18]. The energy loss as a function of incoming energy from the simulations has been fitted to a function $T_{\text{loss}} = aE_{\text{in}}^{b} + c$, where T_{loss} is the total energy loss in the plastic, E_{in} is the incoming energy and a, b and c are coefficients from the fit. This function is used to correct the energy calculated from the time of flight measurement resulting in a plot of the measured energy versus the actual incoming kinetic energy, see Fig. 4.6.

4.3 Results

The calculations of the incoming energies seem to work well. The only run that does not really fit is the 800 A MeV run. It is hard to tell why that is off. It could be that the time calibration is not perfect or that something has changed during the experiment. There were some problems with the POS-detector and it is possible that some changes of settings has caused this. What is a bit more concerning is the misalignment between the 300 and 400 A MeV deuteron runs. As seen in both Fig. 4.5 and 4.6 there is a jump in energy between the two runs. This could also be a result of some change in the settings, possibly in the POS-detector. In the 200 MeV deuteron run there are also one other thing that should be noticed. A second line can be observed at lower incoming proton energies, still depositing approximately the same energies. The working hypothesis of this second line is that it may be caused by deuterons. If the deuterons are slowed down sufficiently, the bending power of the magnet is enough to get also the deuterons into the detector. The reason this line does not match with the other deuteron lines is that these events have been treated as protons in the conversion from time-of-flight to energy, thus getting the wrong energy assigned. When treating these events as deuterons it is found that this line matches the one from the 100 A MeV deuteron sweep run pretty well.

Even though there are some issues of concern the overall result is very satisfying. The energy spectrum shows the expected behaviour with a more or less linear curve for energies up to about 250 MeV, which is a bit low but still reasonable. At this point the energy drops quickly and for higher energies the measured energies drop even more because of the punch-through effect. The most important result is that

a yield factor between the muon energies and the proton energies can be extracted from this data set. When looking at the runs with proton energies below the punch-through energy, and searching for events where both scintillator No. 1 and No. 6 as well as the crystal have been hit, there are hardly any found. Since the energies of the protons impinging on the detector are known and the fact that no punch-through protons are seen, the conclusion must be that the entire energy is absorbed in the detector or that the protons escape through the side of the crystal. That protons hitting the crystal from straight ahead should be scattered out of the side is very unlikely so it can be assumed that most of these non punching through protons are actually stopped in the crystal. The measured energy should thus equal the incoming energy but from Fig. 4.6 it is clear that the measured energy in terms of muon energy units is much less than the actual incoming kinetic energy.

4.4 Outlook

This analysis has been very brief and only provides some preliminary results. As mentioned earlier there are some unexplained effects in the data that need to be investigated carefully. The most obvious at the moment is the energy shift between the 300 and 400 A MeV runs. Comparisons of time of flights between runs with the same settings in the beginning and end of the experiment do not show any differences. Neither does the energy deposition from muons before, during or after the experiment. Thus, so far no explanation to this shift has been found. It should also be found out why the 800 A MeV deuteron run is so far off its calculated time-of-flight position. Also in this case different runs from the beginning and the end of experiment have been compared without revealing any difference. The next step could be to check other time measurements for this energy, e.g. the flight time to the DTF, to the NTF and to the POS++. If also these detectors show similar results, the next step could be to recalibrate the POS detector and the CXB to see if that might improve things. It is also necessary to do some deeper analysis of the 200 A MeV deuteron run to justify the hypothesis that it is slowed down deuterons causing the second line. One more thing that could be improved is the value of the angle between the detector and ALADIN. A change of the angle of one degree gives a change in the calculated energy of 10–15 MeV. The angle used in this analysis is only a simple trigonometric calculation under the assumption that the CXB has been placed behind the centre of paddle No. 5 of the DTF. If it is possible to get a better estimation of the angle from the photogrammetry, this might improve the results.

5 Summary

Nuclear physics experiments often require complex detector systems. Understanding the characteristics of the detectors used is crucial to obtain useful and accurate data. The focus of this thesis has been on two different detectors used in the LAND-setup at GSI: the Crystal Ball and long scintillator bars. The first part of this work focuses on addback routines in the Crystal Ball, i.e. how energies in different crystals should be added to obtain the correct multiplicity and energy of γ-rays and protons. The next chapter treated energy losses in long scintillating bars and the corrections that are necessary to compensate for these losses. The last chapter covers the problem of calibrating the Crystal Ball for proton energies. In the following sections more detailed summaries of each chapter are given.

5.1 Crystal Ball Addback Routines

For low energy γ-rays ($E_\gamma < 4$ MeV) many back-scattered γ-rays can be found (Fig. 2.2 on page 13). These can be used to obtain a high accuracy measurement of the γ-ray energy, but that works well only for single γ-rays. For higher energies the γ-rays are Compton scattered more often and their energy are spread over more crystals, which makes it harder for the addback routines. Protons do not scatter as much and are therefore easier to handle. Although above their punch-through energy ($\sim$ 280 MeV), the detector cannot stop them and thus the entire energy is not deposited inside the detector and it is impossible to determine their total energy. The energy reconstruction of neutrons is very hard. This is mainly due to two reasons, first that they usually do not deposit all their energy inside the detector, and second that they scatter to large angles, if they do interact.

For γ-rays and protons the entire energy is usually deposited however that becomes rarer with increasing energies and especially for protons beyond the punch-through energy (Tab. 2.6 on page 17). Even if the hit is close to the border to another crystal, the highest energy deposition is still in the first hit crystal (Tab. 2.7 on page 18 for γ-rays and Tab. 2.8 on page 18 for protons and neutrons). This is true for γ-rays, protons and neutrons, but in contrast to the γ-rays and protons where the probability drops with increased energies, the probability for neutrons instead increases with increased energy.

For low energy γ-rays the neighbour and bunch routines provided better res-

ults, but with increasing energy the neighbour routine lost some accuracy and for higher energies the second neighbour and bunch routines are superior (Tab. 2.9 on page 22). Also for protons the neighbour and bunch routines are slightly better than the second neighbour routine but here the neighbour routine is better than the second neighbour, also at higher energies (Tab. 2.10 on page 22).

When checking the angular separation capability for the different routines, it is found that the neighbour routine has a separation capability of about 30°, while the second neighbour has a separation capability of about 45° and the bunch routine about 35°. In addition to the original addback routines, some variants with conditions on the number of crystals used in the addback routine $\mathcal{N}$ and back-scattering were tested and also a test with 511 keV signals has been performed. When putting conditions on the addback routine, such as the number of crystals that should be added ($\mathcal{N}$), the correctness for these addback routines increased for low energy γ-rays requiring $\mathcal{N} = 2$ or $\mathcal{N} = 3$. For higher energies no major improvement is seen. On the other hand improvements for higher energy γ-rays are obtained when using crystals with 511 keV deposition while it does not improve the results at lower energies.

5.2 Position Dependence of Energy Signals in Scintillator Bars

Looking at data from different experiments and different detectors, the energy measured in plastic scintillators as used in the LAND-setup, the signal is position dependent. It is largest near the two PMTs. If the energy output is plotted against the position in the detector, the result is a graph looking like a smiley as in Figs. 3.1 on page 28 and 3.6 on page 34. What can also be seen in these figures is that the smiley effect does not reach to the edges but instead drops quite sharp in energy. This has not been considered in the search for corrections in this thesis. The smiley effect originates from reflections of photons at the scintillator surface as described in Eq. 3.2 on page 29. This equation is hard to implement because the needed coefficients are not easily determined. Instead a second degree polynomial can be used. For the LAND detector the polynomial coefficients can be found using cosmic muon data, but for the TFW and NTF another approach is needed. The most efficient way is the use of energy loss spectra of heavy ions from an experimental run. The idea is that all peaks from the different ion species should be found at the same position in the spectra independent of the position of the hit.

To find the coefficients to the correction polynomial, the energy loss-spectra have been plotted for one paddle with the incident ions at different positions.

The quality of the spectra is dependent of the position of the hit, examples are given in Figs. 3.4 on page 32 and 3.5 on page 33. Each peak in the spectra is identified according to its nuclear charge. For each ion a Gaussian fit was applied and this data produced a figure of the smiley effect such as in Fig. 3.6 on page 34. Polynomial fits to each charge provided the coefficients of the second degree polynomial for each ion. By factoring out the constant term from the fit it is possible to obtain a polynomial with coefficients that are independent of the charge of the ion. These coefficients were determined by dividing the first and second order coefficients with the constant term for each charge and using the mean of the values obtained. The corrected energy value can be written in the form provided by Eq. 3.9 on page 39. A check of the quality of this correction, is given by comparing the plots in Figs. 3.8 on page 38 (no correction) and 3.9 on page 39 (correction applied). The result is very satisfactory at lower energies and the correction is improving the energy calibration significantly also at higher energies.

5.3 Muon-Proton Correlation in the Crystal Ball

Calibrating the Crystal Ball for high energies is very challenging. This is mainly due to the lack of sources with sufficiently high energies. To improve this situation a detector called CXB was built. The aim of the detector was to find a relation between the energies deposited in the Crystal Ball by protons and cosmic muons. By knowing this relation it is possible to calibrate the Crystal Ball using cosmic muons. In the data obtained from the experiment, it was found that proton energies are lower than expected. This is seen by the punch through peak in the energy spectrum not beeing found in the 300 A MeV deuteron run as expected from simulation, but in the 400 A MeV deuteron run. The time of flight between the POS and CXB detectors is calibrated using the script called `tcal`. The script cannot handle different offsets which are caused by different cable lengths between the detectors and the data read out. The offset is calibrated using the 200 A MeV deuteron sweep run. Since the distance between the POS and CXB detectors is known, the calibrated time of flight can be converted to energy. The measured energy in the crystal is calibrated with cosmic muons. The path lengths are calculated, and with the knowledge of the energy deposition per length unit for minimum ionising muons, the expected energy deposition is calculated.

After the calibration it is obvious from Fig. 4.6 on page 47 that there is a gain factor between the energy deposition of protons and cosmic muons in the Crystal Ball. To find this gain factor a more thorough analysis is needed. Another topic that also should be investigated is the jump in energy between the 400 A MeV

and 300 A MeV deuteron runs. It is not clear what causes this behaviour, but one hypothesis is that it might have been caused by different settings in the POS detector. Another important thing is to understand why the proton energies are so much lower than expected. Even though many questions are still unanswered, the main result is satisfying. The energy spectrum looks as expected with the punch through peak at a reasonable position and the existence of a gain factor between energies deposited by protons and cosmic muons in the Crystal Ball has been confirmed.

6 References

[1] M. S. Longair, *Theoretical Concepts in Physics: An Alternative View of Theoretical Reasoning in Physics*. Cambridge University Press, 2003.

[2] GSI, "GSI Helmholtzzentrum für Schwerionenforschung," 2011. `http://gsi.de/portrait/ueberblick_e.html`.

[3] W. R. Leo, *Techniques for Nuclear and Particle Physics, A How-to Approach*. Springer-Verlag, 2 ed., 1994.

[4] M. R. Kohan, G. Etaati, N. Ghal-Eh, M. Safari, H. Afarideh, and E. Asadi, "Modelling plastic scintillator response to gamma rays using light transport incorporated FLUKA code," *Applied Radiation and Isotopes*, vol. 70, no. 5, pp. 864–867, 2012.

[5] R. Plag, "Land02 - featuring the unofficial guide to the unofficial version of land02." `http://www-linux.gsi.de/~rplag/land02`.

[6] R. Thies, "Prototype tests and pilot experiments for the R^3B scintillator-based detection systems," Master's thesis, Chalmers University of Technology, 2011.

[7] V. Metag *et al.*, "Physics with 4π–γ–detectors," *Nuclear Physics A*, vol. 409, pp. 331–342, 1983.

[8] K. S. Krane, *Introductory Nuclear Physics*. John Wiley & Sons, 1988.

[9] J. Hykes, "Aluminium-gamma interaction," September 2011.

[10] T. Blaich *et al.*, "A large area detector for high-energy neutrons," *Nuclear Instruments and Methods in Physics Research Section A: Accelerators, Spectrometers, Detectors and Associated Equipment*, vol. 314, no. 1, pp. 136–154, 1992.

[11] R3B-Collaboration, *Technical Report for the Design, Construction and Commissioning of NeuLAND: The High-Resolution Neutron Time-of-Flight Spectrometer for R^3B*, November 2011.

[12] Application Software Group, "Geant, detector description and simulation tool," 1993.

[13] L. Karsch, A. Böhm, K.-T. Brinkmann, L. Demirörs, and M. Pfuff, "Design and test of a large-area scintillation detector for fast neutrons," *Nuclear Instruments and Methods in Physics Research Section A: Accelerators, Spectrometers, Detectors and Associated Equipment*, vol. 460, no. 2–3, pp. 362–367, 2001.

[14] R. Perrino, E. Cisbani, R. D. Leo, *et al.*, "Timing measurements in long rods of BC408 scintillators with small cross-sectional sizes," *Nuclear Instruments and Methods in Physics Research Section A: Accelerators, Spectrometers, Detectors and Associated Equipment*, vol. 381, no. 2–3, pp. 324–329, 1996.

[15] T. Axelsson *et al.*, "Calibration detector for Crystal Ball," *Chalmers University of Technology*, 2012.

[16] P. Adrich, "Some notes about motion of the charged particle through the field of the dipole magnet and the mass measurement with the magnetic spectrometer ALADIN," 2002.

[17] M. Heine. private communication, December 2012.

[18] H. Geissel, C. Scheidenberger, P. Malzacher, J. Kunzendorf, and H. Weick, "Atima." `http://web-docs.gsi.de/~weick/atima/`.

[19] V. Blobel, "Millepede II, Linear Least Squares Fits with a Large Number of Parameters," 2007.

A Appendix

A.1 Correcting the Smiley Effect with Muons

As mentioned in Sec. 3.3, it is possible to use cosmic muons to correct the smiley effect in LAND. This is because its many planes allow calculations of the trajectory of the muon and hence its travelled distance in the scintillator of interest. In the TFW and NTF detectors it is not possible to obtain the trajectory of a muon since those detectors have only two planes. It might still be possible to use the muons for the correction. The scintillators in the two detectors are only 5 mm thick so the path length does not vary that much for muons not originating from straight above. Hence, it would be possible to see the peak from the muons, although it is a bit broader because the path length is not known. By discriminating muons that not hit only one paddle in the x-plane and one in the y-plane, i.e. only use muons which have hit only one paddle in the x-plane and one in the y-plane, the spectra of Fig. A.1 is obtained. The different positions are given by the number of the scintillator that has been hit in coincidence. For example, muons hitting paddle No. 6 in the y-plane and checking what paddle was hit in the x-plane, a rough hit position in the paddle can be obtained.

By looking at the spectra in Fig. A.1 some things can be noticed. The first is that the peaks are not Gaussian shaped and do not seem to move as expected to create the smiley, e.g. the peaks in pos 4 and 5 are almost at the highest position although they are expected to be at the lowest position. Furthermore the count rate is differing quite a lot between the different positions. The largest difference is observed between pos 1 with a bit less than 1000 events and pos 3 which has over 3000 events. Note, that most of the spectra have a sharp edge at lower energies and the peaks seem to be more Gaussian shaped with increased count rate. This is visualised in Fig. A.2 where all the spectra are shown in the same plot. This leads to the conclusion that the energies deposited by the muons are probably close to the thresholds of the CFDs. This means that muons with the shortest path length through the scintillators will not deposit sufficient energy to be measured, and these muons are the ones that distort the peak shape.

From this data one cannot tell if it is possible to use muons to compensate for the smiley effect in the TFW and NTF detectors. Lower thresholds might allow correction of the smiley effect but could potentially also cause triggers from the noise. It is also possible that the dynamic range of the CFD is not sufficient to be able to measure both the low energies of the muons and the higher energies of different ions. This question requires further investigation.

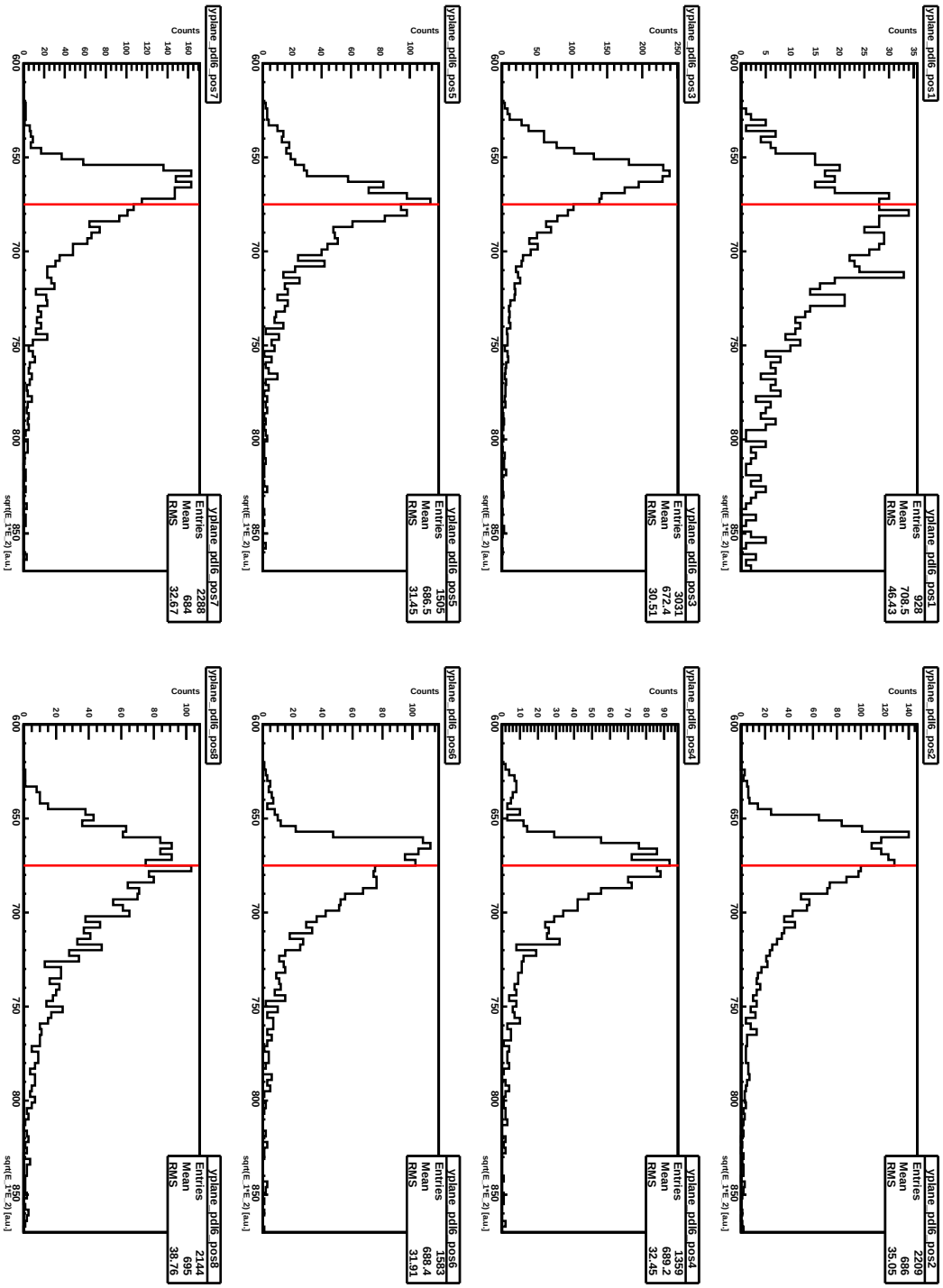

Figure A.1: *The energy spectrum at different positions in paddle No. 6 in the y-plane. The red line is a reference at channel 675 for comparison of the peaks in the different plots. The data is taken from experiment s393, run 306.*

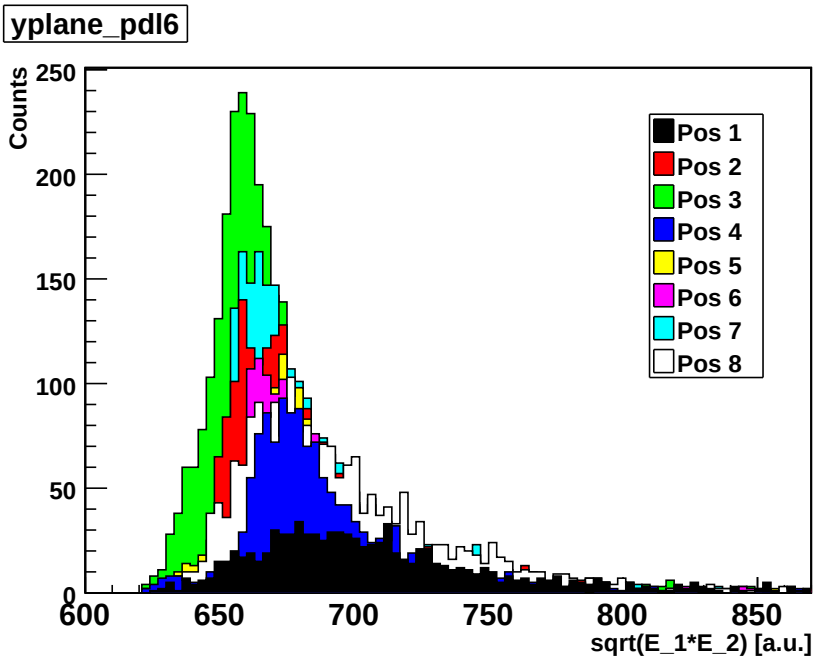

Figure A.2: *The same spectra as in Fig. A.1 but in a common plot.*

A.2 Correcting the Smiley Effect Internally

Another possible method is based on matching the measured energies at each intersection of two paddles. The two paddles measuring the energy deposited by the same ion should measure almost the same energy, except for a minor difference due to the velocity dependence of the Bethe-Bloch formula (Eq. 3.4 on page 31). This calibration is already being done, but at the moment it is only a constant correction while a position dependent correction would be able to correct for the smiley effect. The calibration is made within a script called `phase1`. This script selects events which are characterised as good events using appropriate conditions. These events are used to obtain the difference in energy deposition between two paddles in one intersection. The result for the NTF detector is an 8×8 matrix containing the measured energy difference between the two paddles as elements. The difference in measured energies at each intersection with the constant correction is illustrated in Fig. A.3.

To improve this plot, the constant correction term is replaced for each paddle with a second degree polynomial, $p_0 + p_1 x + p_2 x^2$. Here x is the position of the hit given from the paddle number that has been hit. The origin of this coordinate system is in the centre of the wall. The coefficients p_x are derived for each paddle

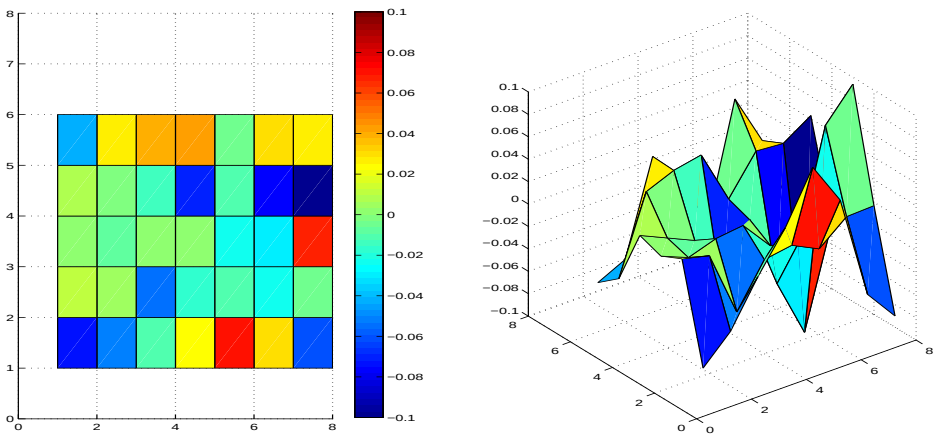

Figure A.3: *The energy difference at each paddle intersection in the NTF given from the script* `phase1` *during experiment s327.*

by solving the over defined linear equation system with each paddle intersection as a measured value. With the NTF having 8×8 paddles one gets a total of 64 intersections and 48 coefficients. After this the problems start. Even though it is an over-defined linear system constraint equations are needed. Some of these are quite easy to find, e.g. it is necessary to prevent a constant shift can be made, i.e. by adding a constant term to all the paddles the energy gain is changed but the difference between two paddles is still the same. This is avoided by requiring that the sum of all zero degree terms has to be zero. It is also necessary to constrain the first degree coefficients. These have to sum to zero in each plane, which gives two more constraint equations. The reason for this is similar to the case of the constant term. Without these constraints it is possible to shift e.g. the linear term and then compensate this with the constant terms in the other plane etc. After this it is more difficult to find further constraint equations. What has to be prevented is e.g. a continuous shift in the linear term in one plane that sums to zero, which can be compensated with another continuous shift in the linear term in the other plane also summing up to zero. When it comes to constraining the second degree term things are even more complicated. In spite of severe effort trying to find the equations needed, no success has been achieved. The necessity of using constraint equations originate from the fact that this approach results in a relative calibration between the paddles, making it possible with many different solutions. To obtain the correct absolute energy it is necessary to calibrate with ions at known energies.

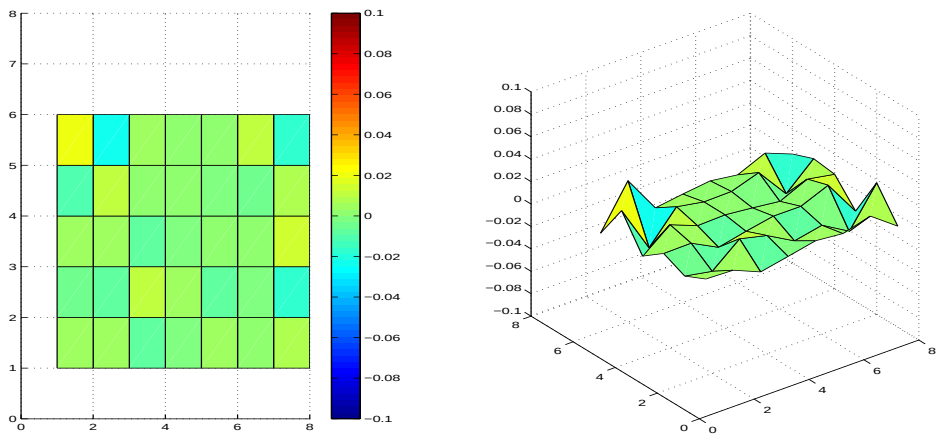

Figure A.4: *The energy difference at each paddle intersection in the NTF given from the script* `phase1` *during experiment s327 when using a polynomial fit.*

Even though the problem is not well defined a general solution can be obtained. If this solution is applied to the problem the plot presented in Fig. A.3 is transformed into the one in Fig. A.4. Only 6×8 paddles are presented because there is insufficient data for the two paddles close to the PMTs.

There is a significant improvement one can see between the two figures. However, if the same method is applied to the TFW the result is not as impressive. The comparison before and after the correction is shown in Fig. A.5. It is not clear why the result differs so much.This could be due to the fact that the correction terms are not well defined and the result depends on the chosen solution. The conclusion is that this method seems to work but before it can be used one has to find the correct constraint equations.

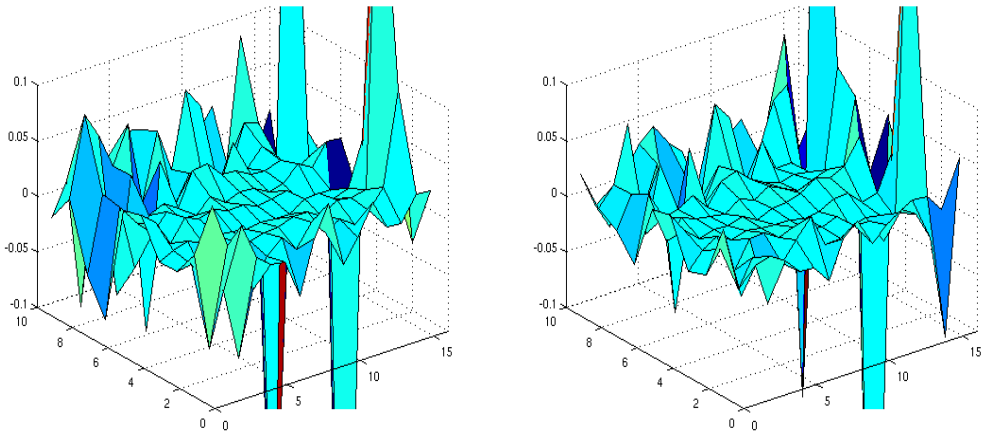

Figure A.5: *The energy difference at each paddle intersection in the TFW given from the script* `phase1` *during experiment s327. The left figure is the original difference and the right figure shows the difference after the correction.*

A.3 Correcting the Smiley Effect Using Millepede

The third solution that was tested is based on the linear equation solving program `Millepede` [19]. It is developed to be able to solve very large equation systems. The program is separated in two different parts, `Mille` which creates a data file and `Pede` which evaluates the data file. What is needed are equations with local variables, which change in each event and global variables which are constant for all events. To be able to solve the equation system `Millepede` needs for every event the residual, i.e. the measured value minus the calculated value, the derivative of both the local and global variables, and the standard deviation of the measurement.

For the problem with the smiley effect the equations were set to

$$E_{\text{meas}} = E_0 \exp\left(\frac{-(\mathrm{L} - x)}{\mathrm{f}(\lambda)}\right)(\mathrm{p}_0 + \mathrm{p}_1 x + \mathrm{p}_2 x^2), \tag{A.1}$$

for each paddle. E_{meas} is the measured energy, E_0 is the deposited energy, the exponential term is the attenuation loss as in Eq. 3.1 on page 27, x is the hit position in the paddle and p_0, p_1 and p_2 are coefficients specific for each paddle. Thus the global variables are $\mathrm{f}(\lambda)$, p_0, p_1 and p_2 and the local variable is E_0. For each event the residual and the derivatives are calculated and stored in a data file. When all the events are evaluated the data file is evaluated by `Pede` to find a solution. Unfortunately the solutions created did not improve the result.

The reason this approach did not work very well is probably the same as for the internal correction. The lack of constraint equations causes the problem to be ill-defined. After some constraint equations were added similar to the ones used for the internal correction, the result improved slightly. If constraint equations could be found and Eq. A.1 is modified to look more like Eq. 3.7 on page 36 this solution might work. However, this task requires considerable effort and is beyond the scope of this work.